

MANIPULATION OF DYNAMICS IN A DROPLET FOR LABEL-FREE DETECTION
OF PROTEINS USING SURFACE-ENHANCED RAMAN SCATTERING AND
PROTEIN MELTING PROFILES

by
Sercan Keskin

Submitted to the Institute of Graduate Studies in
Science and Engineering in partial fulfillment of
the requirements for the degree of
Master of Science
in
Biotechnology

Yeditepe University
2012

MANIPULATION OF DYNAMICS IN A DROPLET FOR LABEL-FREE DETECTION
OF PROTEINS USING SURFACE-ENHANCED RAMAN SCATTERING AND
PROTEIN MELTING PROFILES

APPROVED BY:


Prof. Dr. Mustafa ÇULHA
(Supervisor)



Asst. Prof. Dr. Andrew HARWEY



Prof. Dr. Ertuğrul KILIÇ



DATE OF APPROVAL: / /

ACKNOWLEDGEMENTS

This dissertation would not have been possible without the guidance and the help of several individuals who in one way or another contributed and extended their valuable assistance in the preparation and completion of this study.

Foremost, I would like to express my sincere gratitude to my advisor Prof. Dr. Mustafa Çulha for his continuous support during my master study and research, for his patience, motivation, enthusiasm, and immense knowledge. His guidance helped me in all the time of research and writing of this thesis. I could not have imagined having a better advisor and mentor for my master study.

I would like to give my special thanks to the Yeditepe University Nanobiotechnology former and current group members; Dr. Mehmet Kahraman, Mine Altunbek, Esen Efeoğlu and Dr. Kaan Keçeci for their good advice, support and friendship.

I would also like to thank to other former and current group members; Ertuğ Avcı, Sinan Sabuncu, Sevcan Ayaksız Öztürk, Seda Demir Keleştemur, Şaban Kalay, Zehra Yılmaz, Ali Yasin Sonay, Kemal Keseroğlu, İlknur Sur, İsmail Sayın for their support and friendship.

I want to acknowledge Yeditepe University and TUBITAK for financial support during my master education (Project No: 109T941).

I would like to thank my parents for their love and support throughout my life.

In particular, I would like to thank my beloved girl friend, Esengül, who devoted her energy and love, supporting and encouraging me in every moment of my life. I dedicate this thesis to Esengül with all my love.

ABSTRACT

MANIPULATION OF DYNAMICS IN A DROPLET FOR LABEL-FREE DETECTION OF PROTEINS USING SURFACE-ENHANCED RAMAN SCATTERING AND PROTEIN MELTING PROFILES

Detection and identification of biomacromolecules have critical importance in many fields ranging from biotechnology to medicine. Surface-enhanced Raman scattering (SERS) is an emerging technique for the label-free detection and identification of biological molecules and structures with its fingerprinting properties and high sensitivity. However, there are a number of obstacles for its applications for biological macromolecules due to the complexity of biological samples. In this report, manipulation of microscopic processes in play during the drying of a sessile droplet to influence the nanoparticle-macromolecule packing, which has dramatic effect on SERS performance, before the SERS acquisition is demonstrated. A process known as the “coffee ring phenomenon” jams all particles and molecular species to the edges of the droplet during drying. This uncontrolled process has dramatic effects on a SERS experiment, using colloidal metal nanoparticles as substrates, by sweeping everything to the edges and influencing the packing of nanoparticles in the droplet area.

In this study, the dynamics of silver nanoparticles-protein structures in a drying droplet was explored under two different experimental conditions and the effects of these conditions on SERS performance were investigated. Denaturation profiles of proteins with SERS were also investigated and obtained data was used to detect proteins in multiple protein mixtures. Negatively and positively charged proteins were used as model biomacromolecules in this study. A detection limit of 0.05 $\mu\text{g/mL}$ is obtained for the model proteins with using one of the presented methods.

ÖZET

PROTEİNLERİN İŞARETLEYİCİ MOLEKÜL KULLANMADAN YÜZEYDE ZENGİNLEŞTİRİLMİŞ RAMAN SAÇILMASI VE PROTEİN ERİME PROFİLİ İLE TAYİNİ İÇİN BİR DAMLACIK İÇERİSİNDEKİ DİNAMİKLERİN MANİPÜLASYONU

Biyomakromoleküllerin tanısı ve tayini tıptan biyoteknolojiye kadar bir çok alanda kritik bir öneme sahiptir. Yüzeyde zenginleştirilmiş Raman saçılması (YZRS) “parmak izi” özelliği ve yüksek hassasiyette bir teknik olmasıyla biyolojik moleküllerin işaretleyici molekül kullanmadan tanı ve tayininde kullanılan ve gelişmekte olan bir yöntemdir. Ancak, biyolojik moleküllerin karmaşık yapılarından dolayı, tekniğin uygulanmasında bir takım zorluklar vardır. Bu raporda, yüzey üzerinde kendiliğinden kuruyan bir damlanın içerisinde meydana gelen mikroskopik olaylar amaç doğrultusunda değiştirilmeye çalışılmıştır. Bu değişimin nanoparçacık-makromolekül paketlenmesini ve dolaylı olarak yüzeyde zenginleştirilmiş Raman saçılmasını nasıl etkilediği gösterilmiştir. Damlanın kuruması sırasında gerçekleşen ve “kahve halkası” olayı olarak bilinen süreç damlanın içerisindeki bütün parçacıkları ve molekül türlerini damlanın kenarına sürükler ve o bölgede istif eder. Bu control dışı süreç nanoparçacıkların alt katman olarak kullanıldığı YZRS deneyine, bütün parçacıkları damlanın kenarına sürükleyip nanoparçacıkların paketlenme derecesini belirlemesinden dolayı büyük etki eder.

Bu çalışmada, kuruyan bir damla içerisindeki gümüş nanoparçacık-protein yapılarının dinamiği iki farklı deneysel durum altında araştırıldı ve bu durumların YZRS üzerine etkisi incelendi. Seçilen proteinlerin denatürasyon profilleri YZRS tekniği ile incelendi ve elde edilen veriler çoklu protein karışımlarından protein tespiti için kullanıldı. Negatif ve pozitif yüklü proteinler model biyomakromoleküller olarak kullanıldı. Raporda verilen metodlardan biri ile model proteinlerin tayin sınırı 0.05 µg/mL olarak tespit edildi.

TABLE OF CONTENTS

ACKNOWLEDGEMENTS	iii
ABSTRACT	vi
ÖZET	v
TABLO OF CONTENT	vi
LIST OF FIGURES	viii
LIST OF TABLES	xi
LIST OF SYMBOLS / ABBREVIATIONS	xiii
1. INTRODUCTION	1
2. THEORITICAL BACKGROUND	4
2.1. DETECTION AND IDENTIFICATION OF PROTEINS	4
2.2. PLASMONICS AND PLASMONIC STRUCTURES	5
2.3. RAMAN SCATTERING AND SURFACE-ENHANCED RAMAN SCATTERING AS A PLASMONIC TECHNIQUE	7
2.3.1. Protein Detection with SERS	11
2.4. COFFEE-RING PHENOMENON	12
2.5. PROTEIN DENATURATION AND SERS MEASUREMENTS	13
3. MATERIALS	17
3.1. CHEMICALS	17
3.2. PROTEINS	17
4. METHOD..	19
4.1. PREPARATION OF PROTEIN SOLUTIONS	19
4.2. SYNTHESIS OF SILVER COLLOIDAL SUSPENSION	19
4.3. DYNAMIC LIGHT SCATTERING ANALYSIS	19
4.4. MICROSCOPY	20
4.4.1. SERS Measurement	20
4.4.2. SEM Analysis	20
4.4.3. AFM Analysis	20
4.4.4. THMS600 Heating block and Controllers	20
4.5. SAMPLE PREPARATION	21
4.5.1. A Sessile Drying Droplet	21

4.5.2. Dipping a Plastic Tip into Drying Droplet.....	21
4.5.3. Suspended Drying Droplet against Gravity	22
4.6. HEATINGS of AgNP-PROTEIN SUSPENSIONS	22
5. RESULTS and DISCUSSION.....	23
5.1. SERS MEASUREMENTS OF PROTEINS FROM DRIED DROPLETS	24
5.1.1. SERS Measurements of Droplets with a Tip Dipped during Drying	26
5.1.2. SERS Measurements of Suspended dried Droplets	31
5.1.3. Determining the Detection Limits of the Proteins	38
5.1.4. Denaturation of Proteins with Heat and SERS Measurements.....	41
5.1.4.1. SERS Measurements of Binary Protein mixtures with AgNPs	44
5.1.4.2. SERS Measurements of Ternary Protein mixtures with AgNPs ..	48
6. CONCLUSION and RECOMMENDATIONS	54
6.1. CONCLUSION.....	54
6.2. RECOMMENDATIONS	55
7. REFERENCES	56

LIST OF FIGURES

Figure 1.1. Comparison of different structures in a range from micro to nano-length scale	1
Figure 2.1. Schematic illustration of the LSPR.....	5
Figure 2.2. TEM image of AgNPs obtained by reduction of silver nitrate with sodium citrate.....	7
Figure 2.3. a. Transitional schemes of Raman signal and b. schematic illustration of Rayleigh and Raman scattering	9
Figure 2.4. Schematic illustration of “coffee-ring phenomenon” occurring in a droplet which contains AgNPs and proteins.....	13
Figure 2.5. Levels of structure in proteins	14
Figure 2.6. Schematic illustration of the experimental process	16
Figure 4.1. The heating block under the objectives of Raman Microscopy and the controllers of the heating system.....	21
Figure 5.1. UV/Visible spectrum of 60 nm AgNPs	23
Figure 5.2. Size distribution of AgNPs in the suspension.....	24
Figure 5.3. SEM image of AgNPs.....	24
Figure 5.4. a. Photography of a spot dried from an AgNP-BSA and b. SERS spectra obtained from the different regions of the droplet area. The protein concentration is 500 µg/mL in the droplet.....	25

Figure 5.5. a. Photography of a spot dried from an AgNP-Cyt c and b. SERS spectra obtained from the different regions of the droplet area. The protein concentration is 500 $\mu\text{g}/\text{mL}$	26
Figure 5.6. Photography of a tip dipped droplet on CaF_2 surface	27
Figure 5.7. a. Photography of a droplet area of AgNP-BSA mixture with a tip dipped into the droplet during drying process and b. SERS spectra obtained from the marked regions on the image. Only one spectrum from each region was acquired. The protein concentration is 500 $\mu\text{g}/\text{mL}$..	27
Figure 5.8. a. AFM images obtained from the outermost ring and line analysis of the rings of a droplet dried without and b. with dipping a tip	29
Figure 5.9. a. SERS spectra of BSA from a droplet dried without and b. with a tip dipped during drying. The spectra on both figures were baseline corrected and ten spectra were averaged to obtain each spectrum on the figures	30
Figure 5.10. a. Photographs of droplet areas of AgNP-Cyt c mixture without and b. with a dipped tip and c. SERS spectra obtained from the area of a droplet without a dipped tip and d. with a dipped tip. Ten spectra were averaged to obtain each spectrum on the figures	31
Figure 5.11. Photography of the AgNPs and protein-containing suspended drying droplet on CaF_2 surface.....	32
Figure 5.12. a. Position of AgNPs and b. flow profile of the solvent during drying of a suspended droplet.....	33
Figure 5.13. Comparison of SEM images of droplet areas of AgNP-protein containing droplets. Sessile: a. AgNP-HAS and c. AgNP-Cyt c; suspended: b. AgNP-HAS and d. AgNP-Cyt c. 'M' and 'E' denote	

middle and edge of the droplet area, respectively. Images show a protein concentration of 50 $\mu\text{g/mL}$	34
Figure 5.14. a. AFM images of HSA-AgNP containing sessile and b. suspended dried droplets and c. Cyt-c-AgNP containing sessile and d. suspended dried droplets. The images were obtained from the edges of sessile dried droplets and from the center of suspended dried droplets. The protein concentration of the experiment is 50 $\mu\text{g/mL}$	36
Figure 5.15. SERS spectra of an AgNP-HSA containing suspended dried droplet, a protein-AgNP thin film, a sessile droplet and silver colloidal suspension. The protein concentration of the experiment is 50 $\mu\text{g/mL}$	37
Figure 5.16. a. Ten SERS spectra obtained from negatively and b. positively charged protein containing suspended dried droplets and white light images of the droplet area where these spectra were collected	38
Figure 5.17. SERS spectra of HSA, transferrin, myoglobin, cytochrome c, avidin and lysozyme with their decreasing concentration in AgNP colloidal suspension.....	39
Figure 5.18. Graph of size versus temperature for HSA	42
Figure 5.19. SERS spectra of single proteins at increasing temperatures.....	43
Figure 5.20. a. SERS spectra of HSA, Transferrin and AgNP mixture at increasing temperatures and b. 2D Euclidean Distance plot, TF: Transferrin, HSA: Human Serum Albumin, M: Mixture	45
Figure 5.21. a. SERS spectra of HSA, Mb and AgNP mixture at increasing temperatures and b. 2D Euclidean Distance plot, MB: Myoglobin, HSA: Human Serum Albumin, M: Mixture	46

Figure 5.22. a. SERS spectra of Cyt c, lysozyme and AgNP mixture at increasing temperatures and b. 2D Euclidean Distance plot, CYTC: Cytochrome c, LYZ: Lysozyme, M: Mixture	47
Figure 5.23. a. SERS spectra of Hb, lysozyme and AgNP mixture at increasing temperatures and b. 2D Euclidean Distance plot, HB: Hemoglobin, LYZ: Lysozyme, M: Mixture	48
Figure 5.24. a. SERS spectra of the mixture of HSA, Tf and Mb with AgNPs at increasing temperatures and (b: 30 °C; c: 40 °C; d: 50 °C; e: 60 °C; f: 70 °C) 2D Euclidean Distance plots	49
Figure 5.25. a. SERS spectra of the mixture of HSA, Tf and Hb with AgNPs at increasing temperatures and (b: 30 °C; c: 40 °C; d: 50 °C; e: 60 °C; f: 70 °C) 2D Euclidean Distance plots for each temperature	50
Figure 5.26. a. SERS spectra of the mixture of HSA, Tf and Cyt c with AgNPs at increasing temperatures and (b: 30 °C; c: 40 °C; d: 50 °C; e: 60 °C; f: 70 °C) 2D Euclidean Distance plots for each temperature	52
Figure 5.27. a. SERS spectra of the mixture of Hb, Tf and Cyt c with AgNPs at increasing temperatures and (b: 30 °C; c: 40 °C; d: 50 °C; e: 60 °C; f: 70 °C) 2D Euclidean Distance plots for each temperature	53

LIST OF TABLES

Table 3.1. The physiochemical properties of the proteins in the study	18
Table 5.1. Average Ra values of obtained AFM images	36
Table 5.2. Band assignments for SERS spectra of proteins.....	40
Table 5.3. Melting point values of the proteins in the study.....	42

LIST OF SYMBOLS / ABBREVIATIONS

AFM	Atomic Force Microscopy
AgNP	Silver nanoparticle
AuNP	Gold nanoparticle
BSA	Bovine Serum Albumin
CNT	Carbon nanotubes
Cyt c	cytochrome c
DLS	Dynamic Light Scattering
DNA	Deoxyribonucleic acid
Hb	hemoglobin
HSA	Human Serum Albumin
Hz	Hertz
kDa	kilo Dalton
kV	kilo Volt
LSPR	Localized Surface Plasmon Resonance
LSPs	Localized Surface Plasmons
Mb	myoglobin
min	minute
NASA	National Aeronautics and Space Administration
nm	nanometer
NP	Nanoparticle
PSPs	Propagating Surface Plasmons
QD	Quantum dot
RNA	Ribonucleic acid
SEM	Scanning Electron Microscopy
SERS	Surface Enhanced Raman Scattering
SPs	Surface Plasmons
STM	Scanning Tunneling Microscopy
TEM	Transmission Electron Microscopy
UV/Vis	Ultraviolet/Visible

1. INTRODUCTION

The word of ‘Nano’ means ‘dwarf’ in Greek, and donates a factor of 10^{-9} . It is used as a prefix primarily in the metric system and frequently encountered in science for prefixing units of time and length such as nanoseconds (ns) or nanometer (nm). Nanometer (nm) refers to a length unit of 10^{-9} meter. In order to comprehend this length unit better, Figure 1.1 shows a simple comparison of different natural materials that gives a prior knowledge about the size of matter.

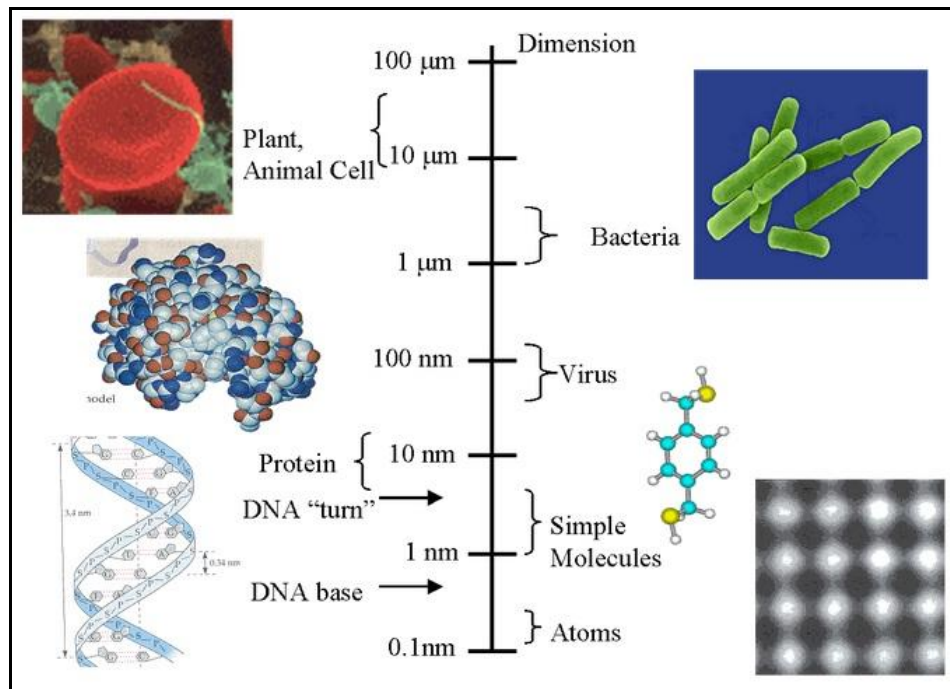


Figure 1.1. Comparison of different structures in a range from micro to nano-length scale

Human beings have unconsciously started to benefit from nanotechnology since ancient times. They realized the interesting features of gold colloids in 4th century B.C. in Egypt [1]. They used gold colloids in steel, glasses and paintings. The Lyscurgus Cup, which is one of the famous examples of these products, was made in 5th century B.C. in Rome.

Michael Faraday is the first scientist who realized the different optic properties of colloidal gold suspension from the bulk material in history. In his experiment, he reduced the

AuCl_4^- by phosphorus in CS_2 and realized that the color of colloidal gold is reddish and different from the color of gold in macro scale. After that, he suggested that there are tiny gold particles in obtained suspension [2]. In 1959, Richard Feynman first suggested the idea of nanoscience with his famous talk “There is plenty of room at the bottom”. He claimed that it was possible to interfere in the materials have size in atomic scale by constructing new compatible tools [3]. The term of “Nanotechnology” was first used by a Japanese scientist from Tokyo Science University, Norio Taniguchi, after 15 years later. In his paper, he defined the term of “Nanotechnology” as “Nano-technology mainly consists of the processing, separation, consolidation, and deformation of materials by one atom or by one molecule.” [4]. Today, this definition was replaced with the common definition of nanotechnology which is “the technology deals with structures sized between 1 and 100 nm”. However, this simple definition is not adequate to define the unique physical properties of nanomaterials. Note that, our macro world has been dominated by Newtonian mechanics. However, when the size of the materials decrease to the nano-scale, the physical laws of Newton are not sufficient to explain the behavior of nanostructures and interaction between them and “Quantum Mechanics come into play” [5]. Therefore, a detailed definition of nanotechnology according to NASA, “The creation of functional materials, devices and systems through control of matter on the nanometer length scale (1-100 nanometers), and exploitation of novel phenomena and properties (physical, chemical, biological, mechanical, electrical...) at that length scale” was accepted. The concept and idea of nanotechnology has further improved by the invention of Scanning Tunneling Microscopy (STM) in 1981. The invention of Atomic Force Microscopy followed after STM and observation of structures in atomic length scale became possible. In recent years, the term of “Nanobiotechnology”, which is considered as a new branch of nanotechnology, has been emerged. It can be considered as the intersection of the terms of nanotechnology and biology and in this field, the approach of nanotechnology to biology allows scientists to create systems that can be used for biological research. Basically, applying the nanostructures or tools to biological molecules, systems or organisms to overcome the relevant problems is the main objective of this field. As it is seen in this thesis, there are components from biology, nanotechnology, physics and chemistry. This thesis explores a novel opportunity to detect and identify an important group of molecules, proteins, by using noble metal nanoparticles showing plasmonic properties as a result of their interaction with light and giving raise an enhancement in Raman scattering. Since the

AgNPs are used as SERS substrate, the behavior of these nanoparticles in a drying droplet is attempted to manipulate to influence their packing density in the droplet area that directly influences the SERS enhancement.

2. THEORETICAL BACKGROUND

2.1. DETECTION AND IDENTIFICATION OF PROTEINS

Proteins as the end product of gene expression are workhorses of living systems that undertake numerous critical processes. Investigation of protein structures, their amino acid sequence, folding/unfolding phenomena and interaction of proteins with other biomolecules are very important in many fields of science and technology. Therefore, their detection, identification and characterization have a vital importance in medicine, biotechnology, and pharmacology.

Mass spectroscopy and immunoassay are the main approaches routinely employed for detection and identification of proteins. Conventionally, proteins are separated with a chromatographic (e.g. HPLC) or an electrophoretic (e.g. CE, 2D PAGE) techniques and then analyzed with mass spectroscopy (MS). Although the unbeatable sensitivity of MS makes the technique attractive for the goal, high cost for instrumentation and requirement for trained personnel are the major issues with the application of the technique [6, 7]. Also, immunoassay based methods such as ELISA, radioimmunoassay, immunosensors and protein microarrays are routinely used techniques for detection of proteins [8, 9]. Even though they offer simplicity and low analysis time, they are problematic, especially, in quantification [10]. The techniques of X-Ray and NMR have to be used in order to determine the detailed 3D structure of a protein.

In addition to the aforementioned techniques above, many PCR assisted immunoassay based approaches were also reported. In a very recent study, a real-time immune-PCR assay was developed for the detection and quantification of a transgenic protein, Cyt1Ab, in the concentration ranged from 100 pg/mL to 100 ng/mL [11]. In another recent study; short RNA fragments called “aptamer”, were combined with immune-PCR (iPCR) and the system was used to detect vascular endothelial growth factor (VEGF). The detection limit of the developed antibody-specific aptamer-based PCR method is over 100 times more sensitive than the original ELISA [12]. Even though these techniques have high sensitivity,

the reliability and applicability of the techniques are limited due to the complexity of the detection systems and very long the protocol execution time.

In following sections, general information about AgNPs and their plasmonic properties are given. Then, the applications of AgNPs, particularly surface enhanced Raman scattering (SERS) are explained and discussed.

2.2. PLASMONICS AND PLASMONIC STRUCTURES

Plasmonics is related to localization and manipulation of electromagnetic waves beyond the diffraction limit and down to the nanometer-length scale [13, 14]. The major components of plasmonics are metal structures since they provide surface plasmon polarization. Surface plasmons occur when electromagnetic waves couple to the collective oscillations of free electrons in the metal. Metallic nanostructures can be differentiated based on the plasmonic modes they support: localized surface plasmons (LSPs) or propagating surface plasmons (PSPs) [15-17]. In LSPs, the electric field associated with the light (E_0) exerts a force on the gas of electrons of the metal and drives them to oscillate collectively. This oscillation will be in resonance with the light at a certain wavelength, which leads to a strong oscillation of the surface electrons. This phenomenon is known as “localized surface plasmon resonance” mode and illustrated in Figure 2.1 [18]. Structures such as spherical AgNPs with a diameter size of 60 nm support LSPR when excited by light as their dimensions are smaller than the wavelength of the light.

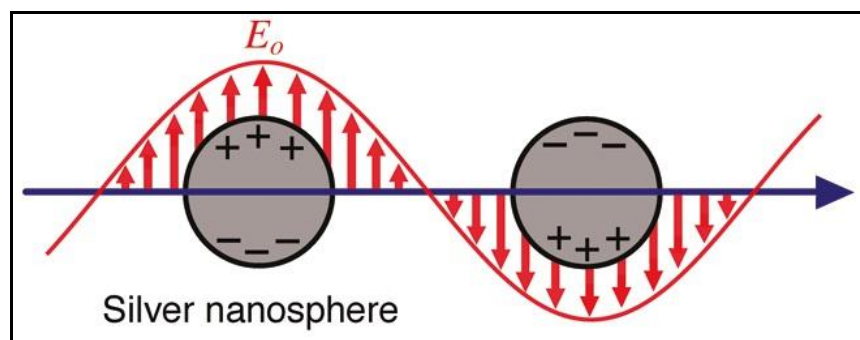


Figure 2.1. Schematic illustration of the LSPR [18]

Plasmonic structures can be used in many spectroscopy techniques such as optical spectroscopy in nanoscale, surface enhanced Raman spectroscopy (SERS) [19], surface Plasmon resonance spectroscopy [17, 20], localized surface plasmon resonance spectroscopy [21]. When plasmonic nanostructures interact with the light, they can both absorb and scatter the light and this property can also be manipulated [22]. Due to this important property, they are used in the fields such as biomedicine, particularly, biophysical studies [23, 24], biomedical detections [25, 26], screening [27-29], medical diagnosis [30], cancer treatment [31-37] in recent years.

Silver is one of the most important plasmonic materials. It has many advantages over Au, Cu, Li and Al and other metals which support surface plasmons in the visible and near-infrared regions [38, 39]. Silver supports SP at the wavelength from 300 nm to 1200 nm. A metallic nanoparticle can support a SP dependent on its dielectric function (ϵ_r). The electric function of a metal reflects the unique interaction between its electrons and the light.

Metallic nanoparticles such as gold (AuNP) and silver (AgNP), carbon nanotubes (CNT) and quantum dots (QD), which are in the range of 1 and 100 nm, are the major groups of these materials that scientists are interested in due to their wide range of applications in optical, electronic and biomedical fields. The physical properties of these nanostructures significantly change based on their size, shape and surface chemistry. Metallic nanoparticles, particularly AgNPs and AuNPs, are used as substrate for SERS due to their plasmonic properties. However, the synthesis methods of these nanoparticles differ, reduction with organic or inorganic agents, ultrasound, UV and Gamma rays [40]. Although the synthesis of NPs in uniform size and shape is challenging, various shapes of AgNPs such as triangular silver nanoplates or nanocubes can be obtained by using different types of reducing agents [41, 42]. They can also be synthesized by microwave-assisted based on the concept of green chemistry [43].

AgNPs can be easily obtained by the reduction of silver nitrate with a reducing agent such as sodium citrate [44]. These nanoparticles are negatively charged due to the citrate adsorption on their surfaces during the synthesis procedure. However, the uniformity of

AgNPs obtained by this method is usually low and they vary in size and shape, as seen in Figure 2.2. The average size of AgNPs prepared with this method is 60 nm.

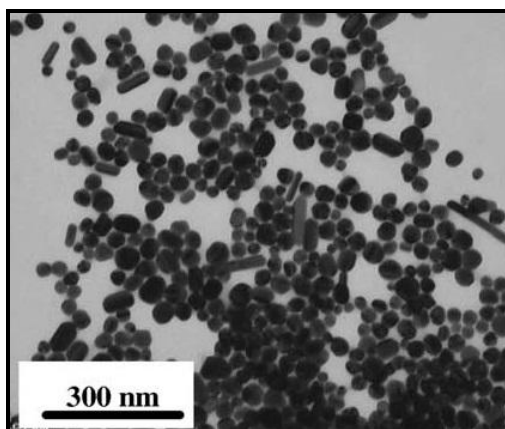


Figure 2.2. TEM image of AgNPs obtained by reduction of silver nitrate with sodium citrate [45]

The AgNPs are also used in other applications other than using them as plasmonic structures. They are known microbial agents and there are many ongoing studies about using AgNPs in the textile and dye industries [46-48]. It was also found that AgNPs could have catalytic activity [49].

2.3. RAMAN SCATTERING AND SURFACE-ENHANCED RAMAN SCATTERING AS A PLASMONIC TECHNIQUE

The Raman scattering is the result of the inelastic collision of photons with molecules. This scattering was first discovered by famous physicist C. V. Raman in 1928. Generally, most of the photons scatter from atoms or molecules at the frequency of the incident radiation. This phenomenon is known as Rayleigh scattering. However, a very small part of this scattering ($1/10^7$) has a frequency (energy) shift from the frequency of the incident radiation by the vibrational energy that is gained (Stokes Raman) or lost (antiStokes Raman) in the molecule. Figure 2.3.a shows the transitional schemes of Raman signal. In Raman scattering, the incident photon interacts with matter and its wavelength can shift to a lower or a higher wavelength. If the final vibrational state of the molecule is more energetic than the initial state, the emitted photon will be shifted to a lower frequency in

order to balance the total energy of the molecule. This shift in frequency is defined as a Stokes shift. If the final vibrational state is less energetic than the initial state, then the emitted photon will be shifted to a higher frequency, and this is defined as an Anti-Stokes shift.

Raman scattering is a two-photon event. In order to obtain Raman scattering, the polarizability of the molecule with respect to its vibrational motion must change. The interaction of the polarizability with the incoming radiation creates a dipole moment in the molecule. The light scattered by the induced dipole of the molecule consists both Rayleigh scattering and Raman scattering [50, 51]. As seen, the top part of Figure 2.3 shows the normal scattering of light, which is Rayleigh scattering. In this process, the light remains at the same energy, however the angle at which the light leaves the molecule can be different from the incident angle. In Raman scattering the process is very similar; however there is one important difference. When the light is scattered from the molecule, it changes the configuration of the molecule slightly. The molecule may rotate or vibrate for instance. Consequently, the electrons oscillate slightly differently and this causes that the light scattered from the molecule has a different energy from the incident light. The scattered light provides a huge amount of information about the molecule and can reflect its exact structure. Since every molecule has a different structure, the Raman spectra can be used to identify the presence of different substances [51].

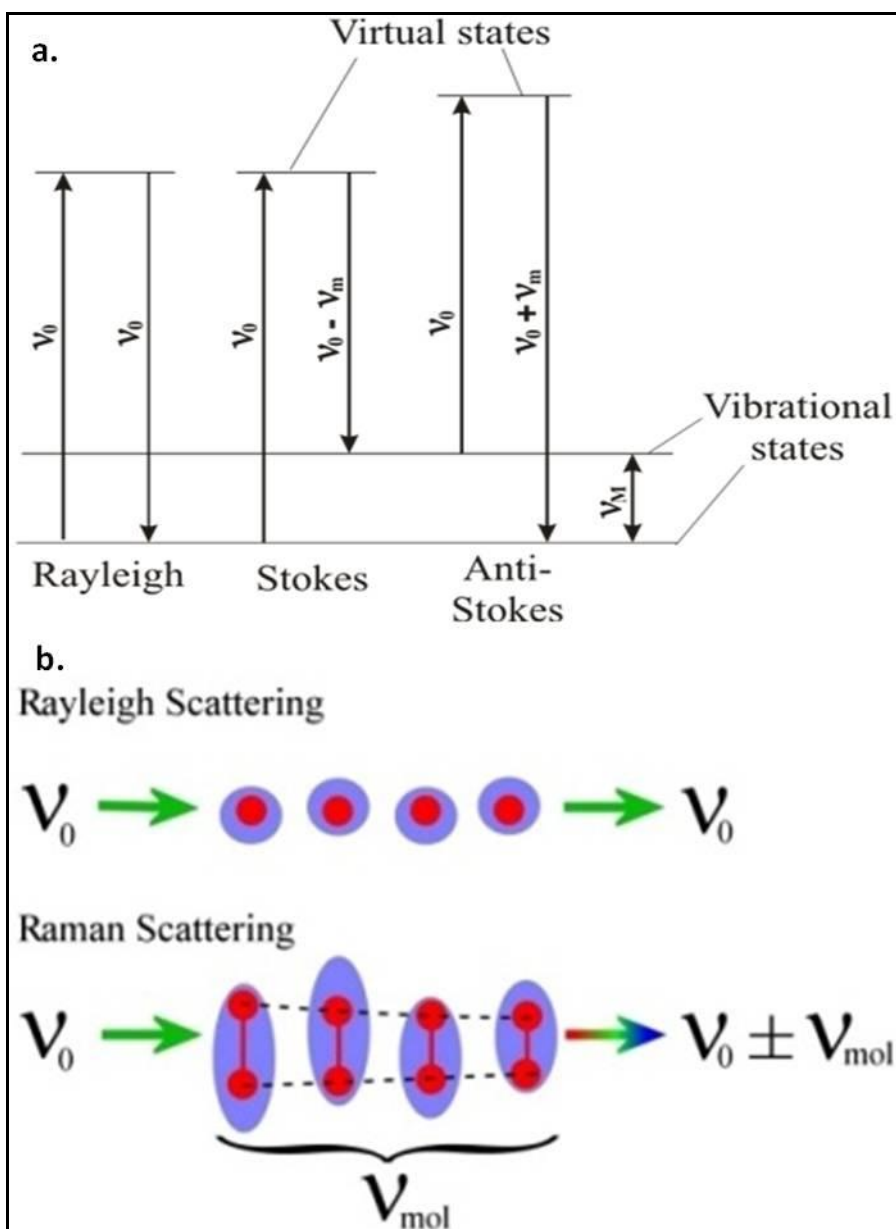


Figure 2.3. a. Transitional schemes of Raman signal and b. schematic illustration of Rayleigh and Raman scattering [52]

A Raman spectrum is a combination of different vibrational modes of the bonds in the molecule. Therefore, it gives information about the chemical structure of the molecule and is considered that the Raman spectrum of a molecule is the “fingerprint” for that molecule. Raman scattering is weak compared to fluorescence and therefore, the measurement of Raman scattering requires a powerful light source and very sensitive detectors [53, 54]. The enhancement of Raman scattering on noble metal surfaces was first observed by

Fleischman et al. in 1974 [55]. This enhancement occurs on the surface of silver, gold, copper, aluminum, indium and platinum and transition metals and emanates from surface plasmon formation and the charge transfer between the metal surface and adsorbed molecule [56-58].

AgNPs have been used as SERS substrates since the early days of the discovery. They have rough surfaces and this has a positive impact on the SERS enhancement. The junctions and groves of the nanostructures, where surface plasmons are localized, provide the optimal enhancement.

In SERS experiments, the detection of the desired molecule can be performed using the molecules intrinsic signature, if reproducible fingerprint information can be obtained from the molecule itself. Otherwise, a reporter molecule must be used to perform the detection indirectly. Small molecules with an aromatic ring or electron rich functional groups can be detected easily without using a reporter molecule. However, large biomolecules with many functional groups generally require a reporter molecule for detection. Therefore, the use of a reporter molecule is preferred, especially for the detection of DNA and proteins that are composed of similar repeating units. In the indirect detection scheme, the reporter molecule is usually a small and Raman active molecule that is chemically or physically linked to one of the molecules in the detection system.

The other important parameter for performing a successful SERS measurement is the distance between the molecule of interest (analyte) and the plasmonic structure such as AgNP or AuNP. The molecule of interest must be in contact to or in close vicinity of the plasmonic structures for a successful SERS measurement. When a small molecule is considered, it is easy to provide appropriate distance as long as the molecule remains in the same location and position near the plasmonic structure. However, when the molecule of interest is a large molecule such as a DNA fragment or a protein, it may not come into contact from all points with the plasmonic nanostructure and the pattern of obtained SERS spectra remains limited to the parts of the molecule, which is interacting with surface of the nanostructure [59-61].

Although SERS has some limitations which arise from the lack of a suitable sample preparation method for all type of molecules and molecular structures, the detection and identification of a number of biological molecules and molecular structures such as proteins [59, 61-63], oligonucleotides, DNA and RNA [64-67], bacteria [68-70], yeast [71], viruses [72, 73] have been reported. There are even examples of the utility of the technique for living cells to gather information about the cellular events taking place in a single living cell [74-76].

2.3.1. Protein Detection with SERS

Detection of proteins can be performed indirectly by using a label that can provide a SERS signature. However, indirect detection has some drawbacks such as extending the duration of the protocol and decreasing the reliability of the detection system [77, 78].

In a report, it was claimed that an assay for label free detection of proteins in solutions was developed [62]. The detection of lysozyme, ribonuclease B, avidin, catalase, and hemoglobin was performed in citrate reduced silver colloidal suspension. The detection limits for lysozyme and catalase as low as 5 $\mu\text{g}/\text{mL}$ and 50 ng/mL , respectively, were achieved. A recent approach involves a heat-induced SERS method using NaNO_3 as an electrolyte for label-free routine and quantitative detection of proteins [79]. In another recent report, the proteins, lysozyme and cytochrome c, were detected by a SERS based biosensor using optical fibers. A detection limit of 0.2 $\mu\text{g}/\text{mL}$ is achieved for both proteins [80].

In order to detect proteins without using an external label, a well-defined sample preparation method is also required. The use of the intrinsic fingerprints of proteins for detection and identification with SERS is highly desired but their diverse surface properties, flexibility, shape and size which define their interaction with the noble metal surface, prevents the development of a universal approach.

Either gold or silver nanostructured surfaces or their colloidal nanoparticles are commonly used as substrates in a SERS experiment. Although both types of substrates suffer from reproducibility issues, the colloidal noble metal nanoparticles are mostly preferred due to

the simplicity of preparation and low cost [81-83]. When a colloidal suspension is used, the analyte is usually mixed with it before spotting on a surface. When colloidal AgNPs or AuNPs are used, many factors influencing the distribution of nanoparticles and analyte in the droplet area, including the charge of the analyte and nanoparticles, and dynamics of the solvent during evaporation from the droplet must be carefully considered. For example, negatively charged analytes in citrate-reduced AgNPs accumulate at the edge of the droplet. However, positively charged analytes co-precipitate in the droplet area with AgNPs [63, 81]. A better understanding of dynamics in a droplet during the drying process will help to design more robust SERS experiments. A phenomenon called “coffee-ring” is responsible from the uneven distribution of species within a dried droplet area [84, 85].

2.4. COFFEE-RING PHENOMENON

The AgNPs are used in this thesis as SERS substrates. When the AgNPs are used as substrates, the sample preparation is as simple as mixing the colloidal suspension with analyte and locating on a surface. As soon as the sample is located on the surface, the coffee-ring phenomenon takes control of the dynamics in the droplet, which is mostly result with the jamming of all species in the droplet at the droplet edge. When a sessile droplet is left to dry at room temperature, all molecular species are forced to the edges of the droplet area due to the outward flow of the solvent. This outward flow arises from a faster evaporation at the edges of the droplet area and due to the loss of the solvent at the edges, the solvent from the middle is generated to consolidate the loss. Therefore, all particles and molecular species in the suspension are dragged and jammed at the droplet peripheral, which is illustrated on Figure 2.4. [84, 85]. This formation is unsuitable for a healthy SERS experiment due to the ineffective oscillation of the nanoparticles' electron systems at the droplet peripheral. In a healthy SERS experiment, controlling the proximity between metallic nanoparticles and analyte molecules is very important for a good SERS enhancement. Analyte used in SERS experiment must be in contact to or in the close vicinity of noble metal surfaces. The optimum distance must be between 1 nm and 3 nm [84-86].

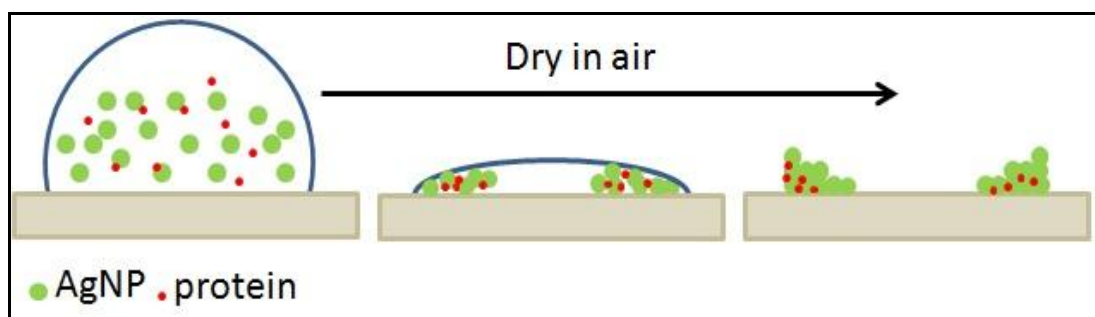


Figure 2.4. Schematic illustration of “coffee-ring phenomenon” occurring in a droplet which contains AgNPs and proteins

In this study, we reported two simple sample preparation methods. The comparison of these methods based on the obtained SERS spectra was provided. In both methods, we can overcome the problems that result with the jamming of all species at the liquid-solid contact of a drying droplet. The first approach demonstrated in the study involves the manipulation of the coffee-ring phenomenon by altering the contact line pinning process by inserting a plastic tip into the drying droplet. The tip inserted into the drying droplet influences the contact line pinning and the distribution of analytes in the droplet area. As the behavior of the nanoparticles is changed, packing of NPs at the liquid-solid contact line is altered, which is critically important for SERS performance. The second approach involves a suspended droplet from a hydrophobic surface altering the dynamics in the droplet during evaporation. The use of a hydrophobic surface prevents the spread of the droplet and keeps the droplet confined as much as possible. The protein-AgNP clusters formed in the middle of the droplet area were found suitable for successful SERS measurements.

2.5. PROTEIN DENATURATION AND SERS MEASUREMENTS

Four levels of protein structure are commonly defined. A description of all covalent bonds (mainly peptide bonds and disulfide bonds) linking amino acid residues in a polypeptide chain is its primary structure. Secondary structure refers to particularly stable arrangements of amino acid residues giving rise to occurring structural patterns such as α -helix or β -sheet. Tertiary structure describes all aspects of the three-dimensional folding of a

polypeptide. When a protein has two or more polypeptide subunits, their arrangement is referred to as quaternary structure. Figure 2.5 shows levels of structure in proteins.

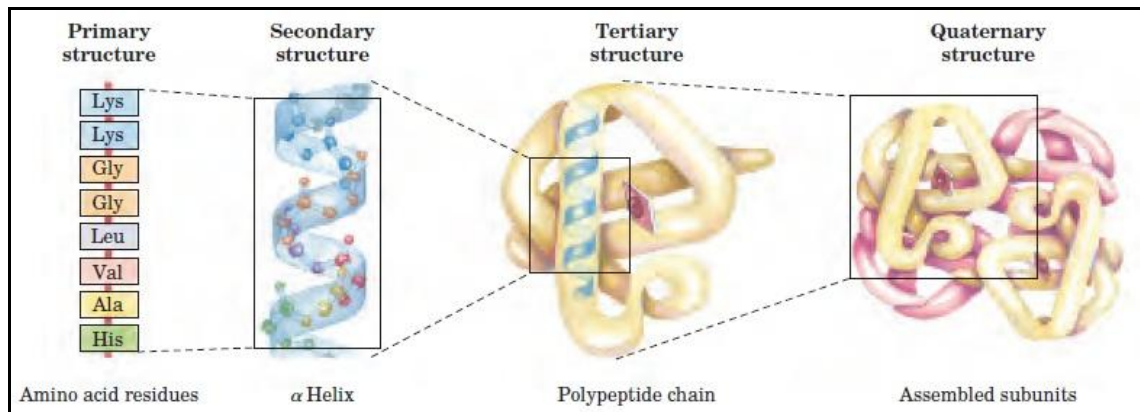


Figure 2.5. Levels of structure in proteins [87]

The conformation of a protein is stabilized mostly by weak interactions. The term stability can be defined as the tendency to maintain a native conformation. The role of these weak interactions is especially important to understanding how polypeptide chains fold into specific secondary and tertiary structures, and how they combine with other polypeptides to form quaternary structures. Individual covalent bonds that contribute to the native conformations of proteins, such as disulfide bonds linking separate parts of a single polypeptide chain, are much stronger than individual weak interactions. However, the weak interactions are more dominant to stabilize the conformation of proteins. In general, the protein conformation with the lowest free energy (that is the most stable conformation) is the one with the maximum number of weak interactions. The hydrogen-bonds of many groups in the polypeptide chain with solvent (water) tend to maintain the unfolded state. The chemical interactions that counteract these effects and stabilize the native conformation include disulfide bonds and the noncovalent interactions. The disulfide-linked residues are strongly hydrophobic (nonpolar). Disulfide bonds play a special role in the structures of many proteins by forming covalent links between parts of a protein molecule or between two different polypeptide chains.

Proteins are very sensitive to heat and in the temperature range of 50-60 °C, most of the globular proteins lose their three dimensional compact structures. This phenomenon is

called denaturation. Most proteins can be denatured by heat, which affects the weak interactions such as noncovalent dipole-dipole interactions between polar amino acid side-chains and the surrounding solvent (primarily hydrogen bonds), covalent interactions between amino acid side-chains (such as disulfide bridges) and Van der Waals interactions between nonpolar amino acid side-chains. Therefore, the structure of the protein becomes an irregular helix. If the temperature further increases, only the covalent bonds between amino acids remain.

In this study, protein-AgNP containing droplets were heated by using a heating system that can be attached to Raman microscopy system. The aim of the study is to enrich the SERS spectra of proteins further and detect and identify them in a multiple protein mixture based on the differences in their denaturation profile. Heat provides an enhancement in Raman scattering, since the electron systems of NPs oscillate more effectively at high temperatures.

Denaturation profiles of the proteins are different and these differences can be reflected on their SERS spectra. It was mentioned that SERS spectrum of a molecule is unique and fingerprint of that molecule. Combination of the fingerprint property of SERS and denaturation profile of proteins provide further sensitivity and reliability to protein detection and identification. Figure 2.6 shows a schematic illustration of the experimental process. There are other parameters that cause protein denaturation rather than temperature, such as organic solvents, UV-radiation, detergents. We selected the parameter of temperature, since addition of another agent into the system further complicates the analysis.

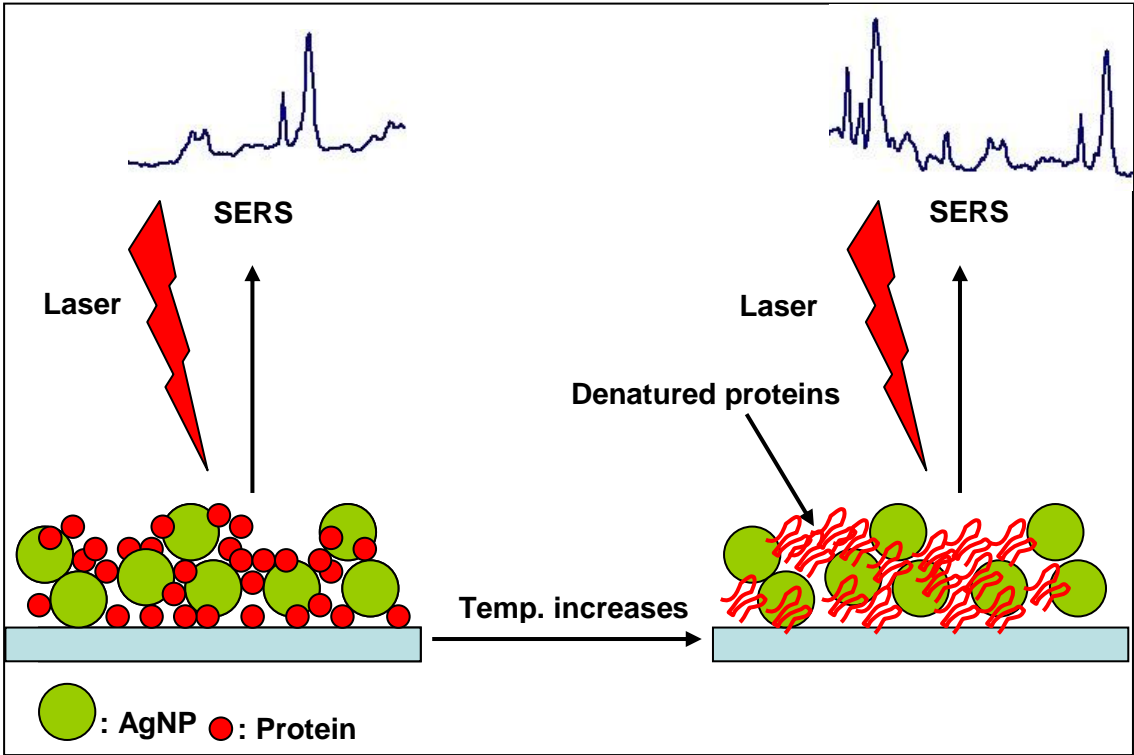


Figure 2.6. Schematic illustration of the experimental process.

3. MATERIALS

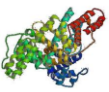




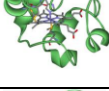
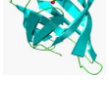
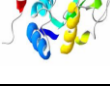
3.1. CHEMICALS

Proteins which used in all experiments were purchased from Sigma Aldrich (Germany). Silver nitrate (AgNO_3) was purchased from Fluka (Germany) and sodium citrate ($\text{NaH}_2\text{C}_6\text{H}_5\text{O}_7$) was purchased from Merck (Germany). Ultra pure water (Millipore, Direct Q-UV) was used to dissolve proteins and prepare protein stock solutions.

3.2. PROTEINS

Five acidic, Bovine serum albumin (BSA), human serum albumin (HSA), transferrin (Tf), myoglobin (Mb), hemoglobin (Hb) and three basic, cytochrome c (Cyt c), avidin and lysozyme (LYZ), proteins were used in the study. The proteins were selected by considering basically the charge they carry and the size they have. The physiochemical properties and structures of selected proteins were shown on the Table 3.1. Dynamic Light Scattering (ZetaSizer) was used to find the properties of hydrodynamic radius and zeta potential of the proteins.

Table 3.1. The physiochemical properties and structures of the proteins in the study

Protein	Isoelectric point (pI)	Molecular weight (kDa)	Zeta potential (mV)	Hydrodynamic radius (nm)	Property	Structure
BSA	4.7-4.9	66.4	-22.7	8.019	Acidic	
HSA	4.7-5.2	66.5	-28.9	7.937	Acidic	
Tf	5.5	76	-18.4	15.55	Acidic	
Mb	6.8-7.3	17.6	-17.6	4.259	Acidic	
Hb	6.8	64.5	-13	8.911	Acidic	
Cyt c	10-10.5	12.3	+22.5	2.01	Basic	
Avidin	10	66	+27.1	3.53	Basic	
Lyz	11.4	14.3	+25.9	2.1	Basic	

4. METHOD

4.1. PREPARATION OF PROTEIN SOLUTIONS

Protein stock solutions were prepared by using lyophilized proteins and the concentration of each protein stock solution were set as 1 mg/mL. 100, 10, 1 and 0,1 $\mu\text{g/mL}$ protein solutions were prepared by diluting the protein stock solutions.

4.2. SYNTHESIS OF SILVER COLLOIDAL SUSPENSION

The AgNPs were synthesized by using the method reported by Lee and Meisel [44]. 90 mg of AgNO_3 was dissolved in 500 ml distilled H_2O and heated until boiling. A volume of 10 mL of 1 per cent trisodium-citrate solution was added drop wise to reduce Ag^+ ions to AgNPs. The solution was kept boiling until the volume was reduced to 250 mL (approximately, half of the initial volume). Then, the solution was kept at the room temperature until cooling. The suspension was filtered with a 0.22 μm filter to remove large aggregates. This suspension is called 1X. The synthesized colloidal AgNPs were characterized with scanning electron microscopy (SEM), DLS (Zetasizer) and UV/vis Spectroscopy. The 1X AgNP suspension was centrifuged (Beckman, Rotor: S4180) at 5500 rpm for 30 min and a portion of supernatant was removed from to bring the final concentration of AgNP suspension to 8X.

4.3. DYNAMIC LIGHT SCATTERING ANALYSIS

The size and zeta potential analysis of the proteins and nanoparticles were performed using Zetasizer NanoZS (Malvern, UK) at 25 $^\circ\text{C}$. It contains a 4 mW He-Ne laser with a wavelength of 633 nm. The scattered light was collected by an avalanche photodiode detector with an angle of 173° . The refractive index and absorption of the protein solutions were assumed as 1.45 and 0.001, respectively.

4.4. MICROSCOPY

4.4.1. SERS Measurement

A Raman Microscopy System (InVia Reflex, Renishaw, UK) was used to perform all SERS experiments. The system was used with a diode laser at 830 nm and 50X objectives. The 50X long-range objective was used with the heating system (THMS600) to prevent the objective from any damage caused by high temperature. The system was automatically calibrated against a silicon wafer peak at 520 cm^{-1} . The laser power of 3 mW was used for the measurements at room temperature and the laser power of 15 mW was used for the analysis of protein melting profiles. The exposure time for each SERS measurement was 10 s. The spectra were processed with WIRE 3.2 software provided by Renishaw.

4.4.2. SEM Analysis

All SEM images were obtained by using a Carl Zeiss Evo 40 instrument under high vacuum and high potential (10 kV).

4.4.3. AFM Analysis

The AFM (Park Systems XE-100, Korea) images were obtained in non-contact mode at room temperature. Silicon nitride tips were used with varying resonance frequencies at a linear scanning rate of 0.5 Hz.

4.4.4. THMS600 Heating block and Controllers

THMS600 heating system was fixed to Raman Microscopy system by placing the heating block under the microscope objective, which can be seen on Figure 4.1. It can heat the sample until $600\text{ }^{\circ}\text{C}$ and cool it until $-195\text{ }^{\circ}\text{C}$.

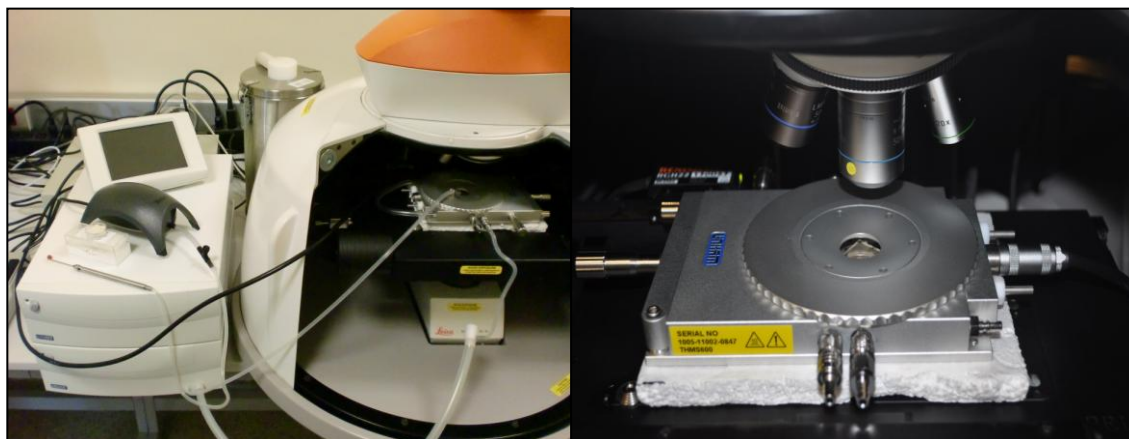


Figure 4.1. The heating block under the objectives of Raman Microscopy and the controllers of the heating system

4.5. SAMPLE PREPARATION

Equal volume of protein solutions with various concentrations of 100, 10, 1, 0.1 $\mu\text{g}/\text{mL}$ were mixed with 8X silver colloidal suspension to bring the final protein concentration to 50, 5, 0.5 and 0.05 $\mu\text{g}/\text{mL}$, respectively. 2 μL of this protein-AgNP mixture was spotted on a CaF_2 surface. It is a hydrophobic surface which resembles a basic glass slide and prevents the molecular species in drying droplet from spreading through the surface.

4.5.1. A Sessile Drying Droplet

A 2 μL of protein-AgNP mixture was spotted on a CaF_2 surface and left to dry at room temperature. The room temperature and relative humidity were 22-25 $^{\circ}\text{C}$ and 40-50 per cent during the experiments, respectively.

4.5.2. Dipping a Plastic Tip into a Drying Droplet

After spotting 2 μL of protein-AgNP mixture on CaF_2 surface, a plastic tip with 200 μm radius was dipped into the droplet possessing radius of 1400 μm placed on the surface and left to dry until complete dryness at room temperature.

4.5.3. Suspended Drying Droplet against Gravity

A volume of 2 μL protein and colloidal AgNP mixture was spotted on a CaF_2 slide. Then, the CaF_2 slide was fixed to a clamp at the overturned position with an angle of 180 degrees around its own axis. The position of the clamp was maintained until the droplet completely dried at room temperature.

4.6. HEATING of AgNP-PROTEIN SUSPENSIONS

After spotting 2 μL of protein and AgNP mixture on CaF_2 slide and dried with selected configuration, it placed on the heating block of THMS600 system. The temperature of the system was set as 30 $^\circ\text{C}$ and increased until 70 $^\circ\text{C}$ with 10 $^\circ\text{C}$ intervals. The period of waiting between two consecutive temperatures was set as 90 s in order to the temperature of the environment reaches the temperature of the heating block. Five SERS spectra were collected from different spots and averaged to one spectrum for each temperature.

5. RESULTS and DISCUSSION

The AgNPs with approximately 60 nm diameter in size were used in SERS measurements due to their simple synthesis procedure and strong plasmonic properties. Figure 5.1 and Figure 5.2 show UV/Visible spectrum and DLS plot, respectively, which give information about the size distribution of AgNPs in the suspension. The maximum absorption of 60 nm AgNP suspension is 420 nm. DLS measurement can give information about the hydrodynamic radius of particles rather than their real diameter values due to the working principle of the device. The DLS plot indicates that the size of AgNPs in the suspension is uniform enough to perform the SERS experiments. The most reliable information about the size of AgNPs can be obtained from electron microscopy. Figure 5.3 shows a SEM image of AgNPs which support the previously obtained data from UV/vis spectrum and DLS plot.

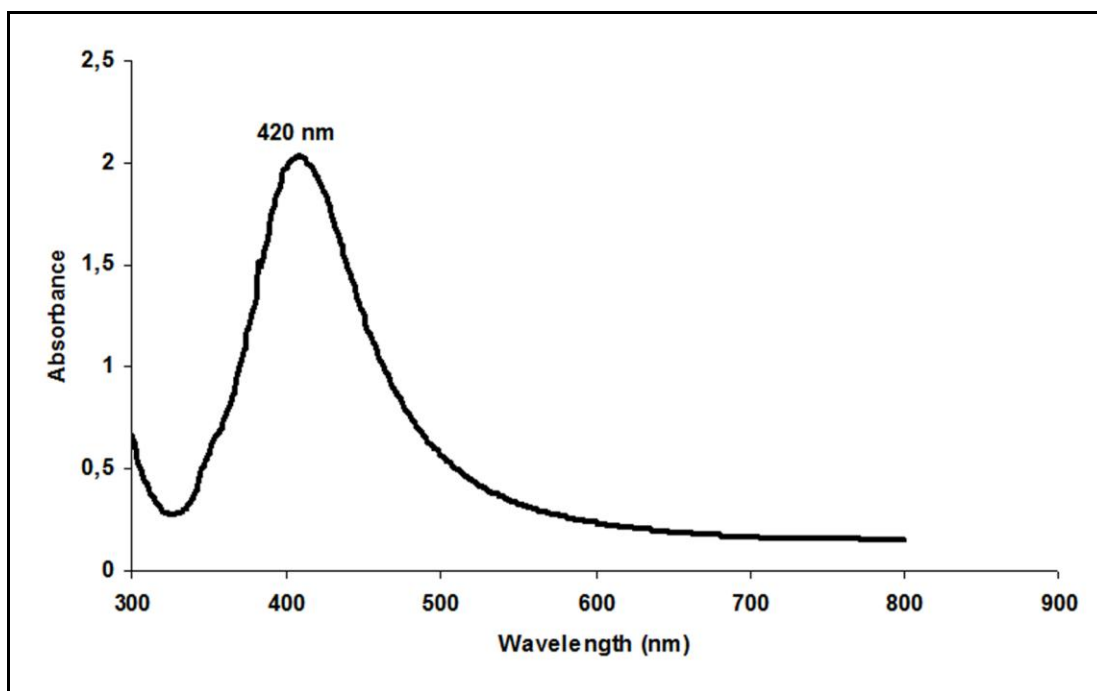


Figure 5.1. UV/Visible spectrum of 60 nm AgNPs

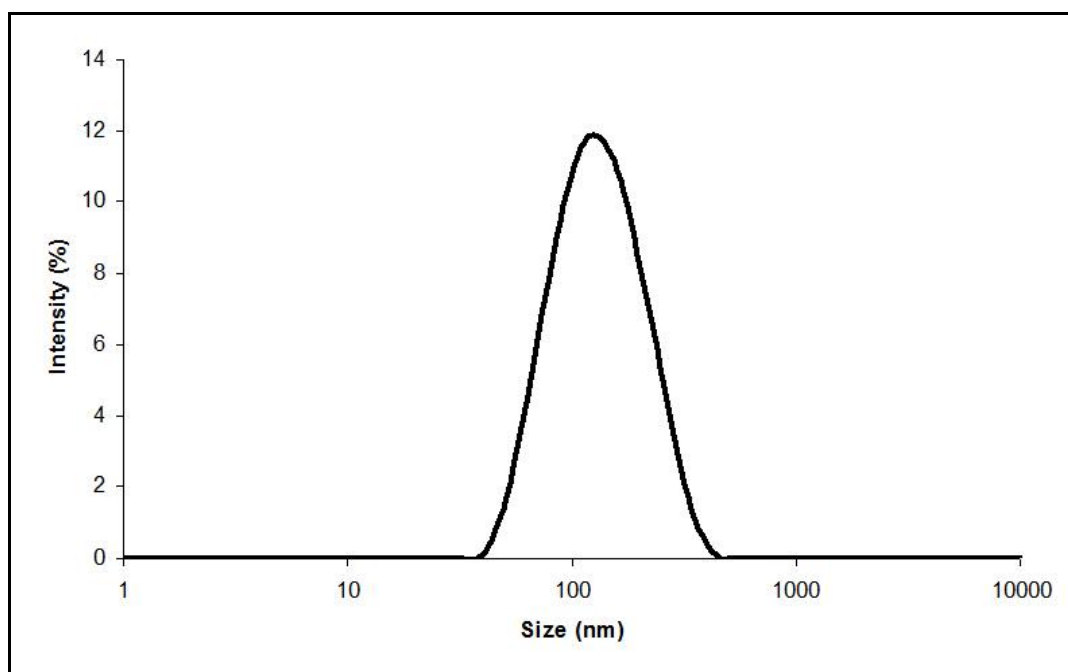


Figure 5.2. Size distribution of AgNPs in the suspension

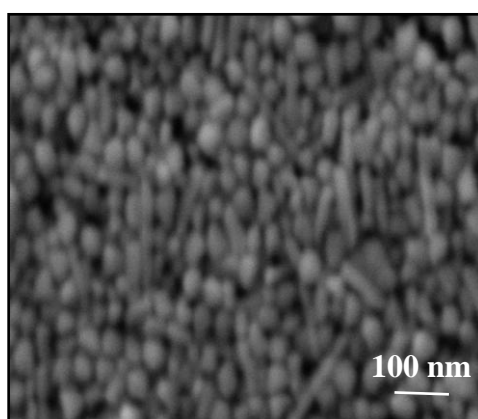


Figure 5.3. SEM image of AgNPs

5.1. SERS MEASUREMENTS OF PROTEINS FROM DRIED DROPLETS

Figure 5.4.a and Figure 5.4.b show a white light image of a spot dried from an AgNP-BSA and SERS spectra obtained from the different regions of the droplet area, respectively.

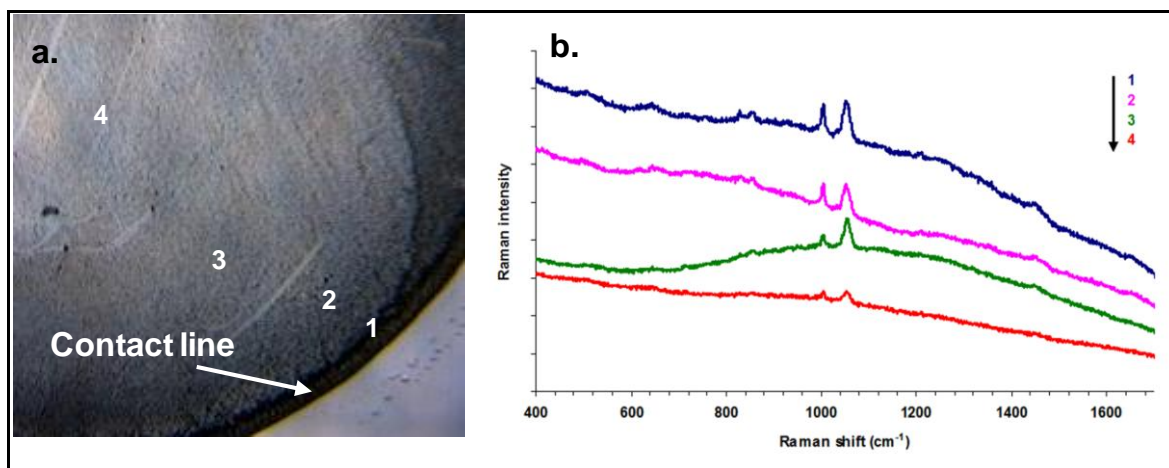


Figure 5.4. a. Photography of a spot dried from an AgNP-BSA, b. the SERS spectra obtained from the different regions of the droplet area. The protein concentration is 500 $\mu\text{g/mL}$ in the droplet

The charge of the analyte molecules strongly influences the interaction with metallic nanoparticles. The AgNPs are negatively charged due to the adsorption of citrate ions on their surfaces. Therefore, when a negatively charged protein and AgNP suspension is mixed and spotted on a surface, due to the weak interaction between NPs and protein molecules, a poor SERS spectrum is obtained, which can be seen on Figure 5.4.a. As seen, most of the AgNPs along with the BSA molecules are piled up at the edge of the droplet due to the coffee-ring phenomenon. This uncontrolled piling results in tightly packed AgNPs-BSA conjugates, which is not a proper structure for surface plasmon formation [86, 87]. The amount of AgNP-BSA aggregates is much less in the rest of the droplet area, as seen on the image. Therefore, the quality of the SERS spectra further decreases towards the middle of the droplet area due to an insufficient amount of protein molecules to detect by using SERS.

When a positively charged protein is used in the same experiment, the ionic interaction between metallic NPs and protein molecules causes an improvement in the SERS enhancement. Figure 5.5.a and Figure 5.5.b show a white light image of a spot dried from an AgNP-Cyt c and SERS spectra obtained from the different regions of the droplet area, respectively. As seen, AgNPs and Cyt c molecules show a more homogenous distribution

compared to a negatively charged protein and AgNP containing sessile dried droplet and the quality of the SERS spectra is very similar through the droplet area for Cyt c.

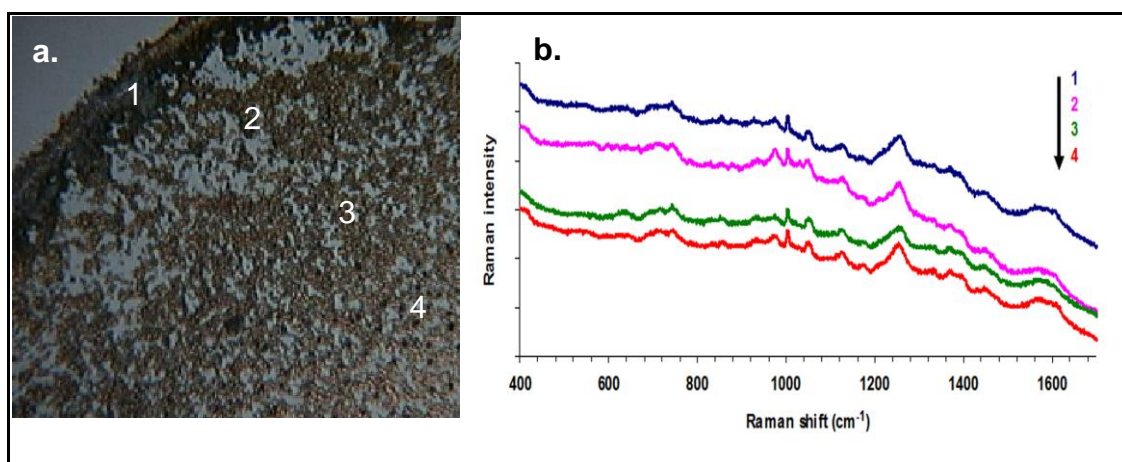


Figure 5.5. a. Photography of a spot dried from an AgNP-Cyt c and b. SERS spectra obtained from the different regions of the droplet area. The protein concentration is 500 $\mu\text{g/mL}$

The spectral quality is not satisfactory for protein detection in low concentrations without using an external molecular label. A simple and effective approach is needed to alter the behavior of AgNP-protein conjugates in a droplet.

5.1.1. SERS Measurements of Droplets with a Tip Dipped during Drying

The first approach used in the study involves dipping a plastic tip into the droplet as soon as it is placed on a surface for drying. Figure 5.6 shows photography of a tip dipped droplet on a CaF₂ surface.

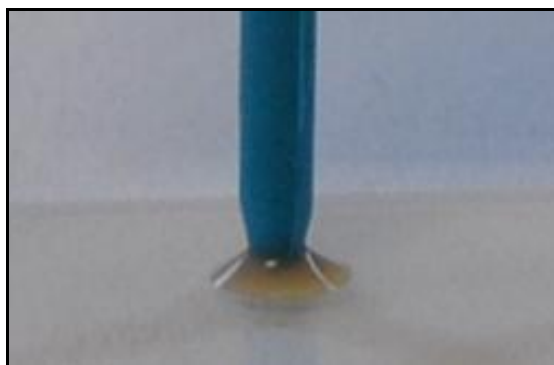


Figure 5.6. Photography of a tip dipped droplet on CaF_2 surface

Figure 5.7.a and Figure 5.7.b show the area of a droplet containing AgNP-BSA generated by a dipped-tip and the SERS spectra obtained from the marked regions, respectively. The formation of the consecutive rings indicates that the contact line moves during the drying process and this movement is explained with the slip-stick motion of the contact line [88-91]. As compared to a sessile droplet, the AgNPs and protein molecules are distributed in a more controlled manner with the insertion of a tip, which has a considerable effect on the AgNP-protein packing. This effect is reflected to the SERS spectra. As seen on Figure 5.7.b, the quality of the SERS spectra increases significantly and new Raman bands appear compared to the spectra obtained from a sessile dried droplet.

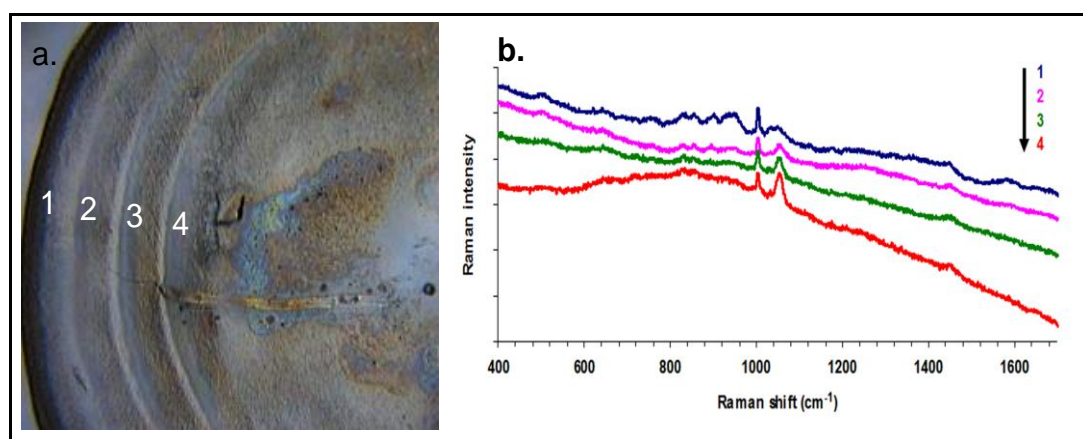


Figure 5.7. a Photography of a droplet area of AgNP-BSA mixture with a tip dipped into the droplet during drying process and b. SERS spectra obtained from the marked regions on the image. Only one spectrum from each region was acquired. The protein concentration is 500 $\mu\text{g}/\text{mL}$

Figure 5.8.a and Figure 5.8.b show the AFM images obtained from the outermost ring and line analysis of the rings of a droplet dried without and with dipping a tip, respectively. The line analysis provides information about the packing density of AgNPs-protein conjugates. The parameter indicating the surface roughness (Ra) is in the range of 5-10 for the droplet dried in the absence of a tip and is in the range of 19-23 in the presence of a dipped tip. This indicates that the packing density of AgNP-protein structure is higher in the absence and lower in the presence of the tip. This means that the oscillations of electron system of loosely packed AgNP structures will be much more effective and this will lead the improved SERS activity.

The detection limit of two proteins, BSA and Cyt c, was also investigated by decreasing the concentration of the proteins in the colloidal AgNP suspension. Figure 5.9 shows a comparison of the SERS spectra obtained from a sessile dried and a tip dipped dried droplets. It is obvious that the quality of the SERS spectra obtained from a tip dipped droplet is better than the quality of the SERS spectra obtained from a sessile dried droplet. While the spectral features disappear at the lowest concentration of BSA, 5 $\mu\text{g/L}$, without a tip dipping, the features are still apparent at this concentration level with a dipped tip.

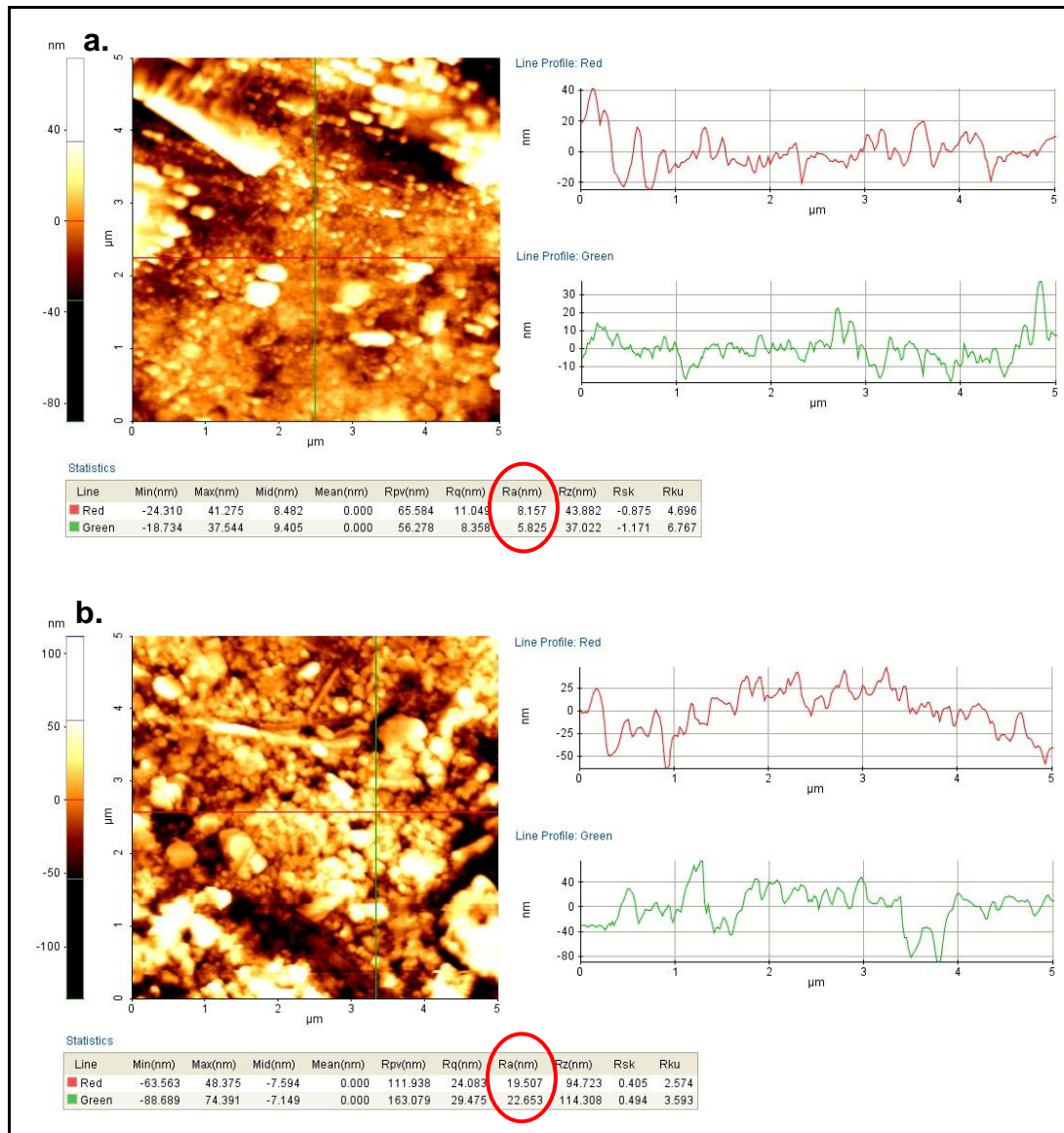


Figure 5.8. a. AFM images obtained from the outermost ring and line analysis of the rings of a droplet dried without and b. with dipping a tip

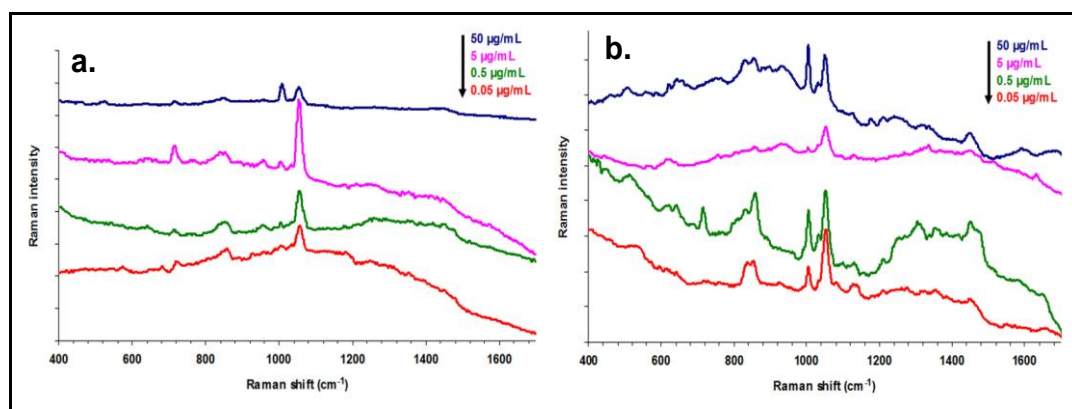


Figure 5.9. a. SERS spectra of BSA from a droplet dried without and with b. a tip dipped during drying. The spectra on both figures were baseline corrected and ten spectra were averaged to obtain each spectrum on the figures

The same experiment was repeated using the positively charged protein, Cyt c. The charge of the analyte has an important effect on the distribution of AgNPs and analyte molecules throughout the droplet area for both sessile and tip dipped drying droplets. Although, the similar slip-stick motion was observed in the tip dipped, negatively or positively charged protein containing drying droplets, the pattern and quality of the SERS spectra obtained from both a sessile and a tip dipped, positively charged protein containing dried droplets do not have a significant difference. Figure 5.10.a to 5.10.d show the photographs of droplet areas of AgNP-Cyt c mixture without and with a dipped tip and SERS spectra obtained from the area of a droplet without a dipped tip and with a dipped tip. Ten SERS spectra were randomly collected from the whole area of a droplet without tip dipped and from the ring region of a droplet with a dipped tip and averaged to one spectrum for each different protein concentrations. The ring region was preferred for a tip dipped droplet since it was found the most suitable region for a healthy SERS measurement.

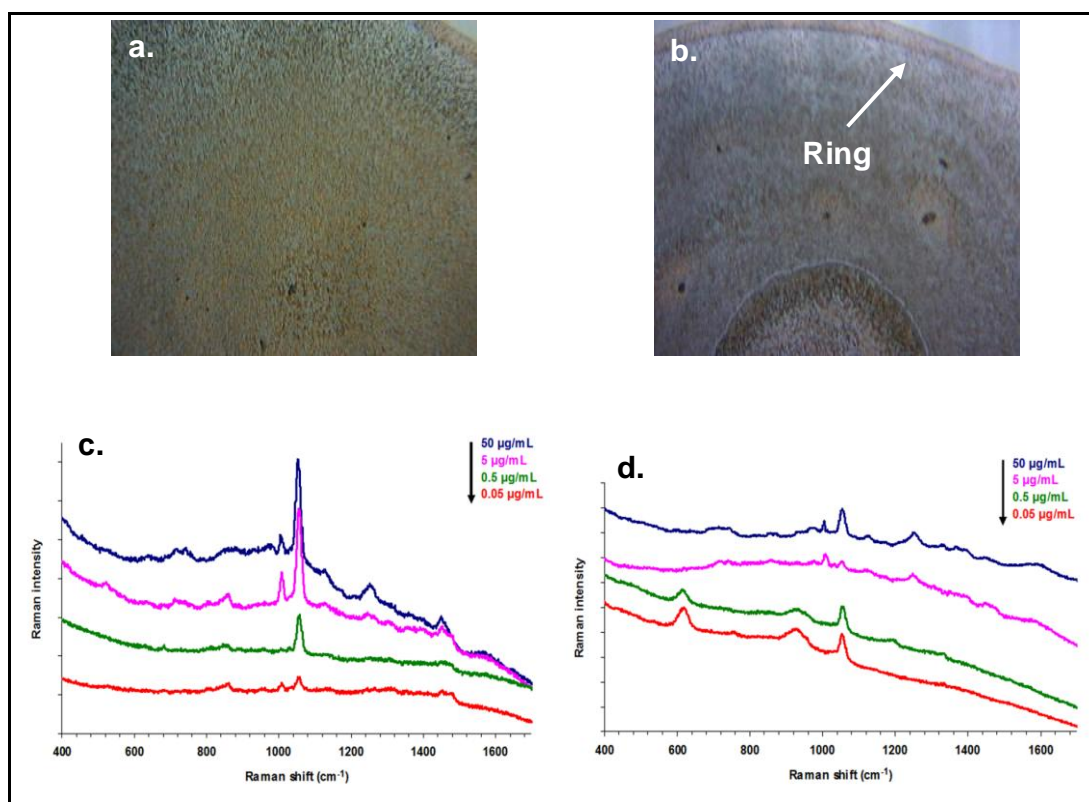


Figure 5.10. a. Photographs of droplet areas of AgNP-Cyt c mixture without and b. with a dipped tip and c. SERS spectra obtained from the area of a droplet without a dipped tip and d. with a dipped tip. Ten spectra were averaged to obtain each spectrum on the figures

Although the demonstrated approach is very simple, the effectiveness on the SERS performance is not satisfactory, particularly for positively charged analyte molecules. Simply dipping a tip into a drying droplet can improve the detection limit of negatively charged biomacromolecules more than one order of magnitude.

5.1.2. SERS Measurements of Suspended Dried Droplets

The second approach which was used to manipulate the distribution of AgNPs and proteins involves suspending a droplet from a hydrophobic surface during drying at room temperature. Figure 5.11 shows the photograph of a suspended drying droplet from CaF₂ surface.

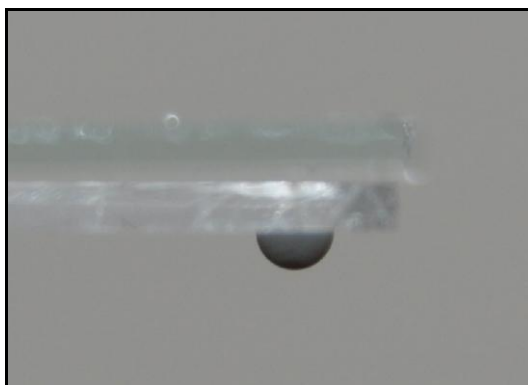


Figure 5.11. Photography of the AgNPs and protein-containing suspended drying droplet on CaF_2 surface

When a suspended droplet is dried at room temperature, all particles, which have varying size and weight is forced to accumulate in the middle of the droplet area due to the gravity. This process is similar to the process proceeding in a sessile droplet, due to greater evaporation rate at the solid-liquid contact line of the droplet, a solvent flow is generated from the center of the droplet towards to the edges as the contact line is pinned. This solvent flow exerts a force to drag the accumulated species from the middle of the droplet to the edges. However, this force is not powerful enough to drag the accumulated heavy particles and molecular species at the tip of the overturned droplet. Therefore, only small and freely suspended nanoparticles and molecules remained dissolved and unattached to the accumulated aggregates are dragged to the edges. Figure 5.12.a and 5.12.b show the position of AgNPs and flow profile of the solvent during drying of a suspended droplet, respectively. The heavier AgNP-protein aggregates tend to accumulate in the middle of the droplet area. The solvent flow of the droplet continues during drying and drags any species either dissolved or suspended in the liquid and jams at the contact line. Some of the AgNP-protein structures are accumulated at the tip of the droplet, they can escape from the outward flow. Figure 5.13.a to 5.13.d show the SEM images of dried droplet areas for both proteins at two different configurations. The images denoted as “M” and “E” shows the middle region and the edge of droplet, respectively, given on the left. As seen on Figure 5.13.a, the majority of the AgNP-HSA hybrid structures are jammed at the edges while some aggregates remain scattered in the rest of droplet area depending on the protein and nanoparticle concentration. Note that the AgNP-protein structures neither at the edges nor in the droplet area of a sessile dried droplet are favorable for healthy SERS measurements.

When the droplet is dried suspended, this profile significantly changes and AgNP-HSA hybrid structures significantly accumulate in the middle of the droplet area. Figure 5.13.c shows the SEM image of the droplet area of a suspension droplet containing AgNP-Cyt c. Since the AgNPs are negatively charged, the positively charged Cyt c strongly interacts with the AgNPs and precipitate in the droplet area escaping from the coffee-ring phenomenon. When the droplet is suspended, the majority of the AgNP-Cyt c accumulates in the middle of the droplet. However, there are still small portions of free protein molecules and nanoparticles visible at the edge of the droplet area. Therefore, when the droplet is dried in air in the suspended position, a similar pattern for both negatively and positively charged proteins is observed with most of the AgNP-protein structures accumulated in the middle of the droplet area.

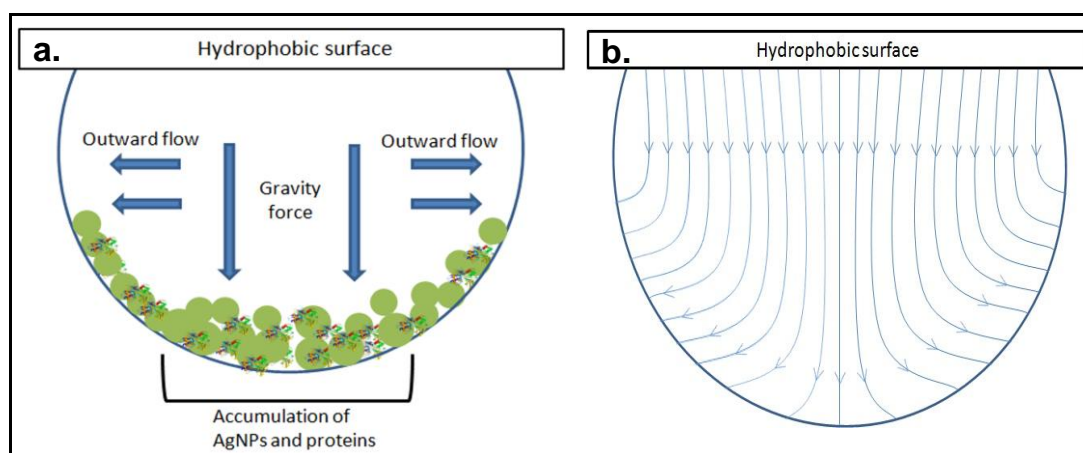


Figure 5.12. a. The position of AgNPs and b. flow profile of the solvent during drying of a suspended droplet

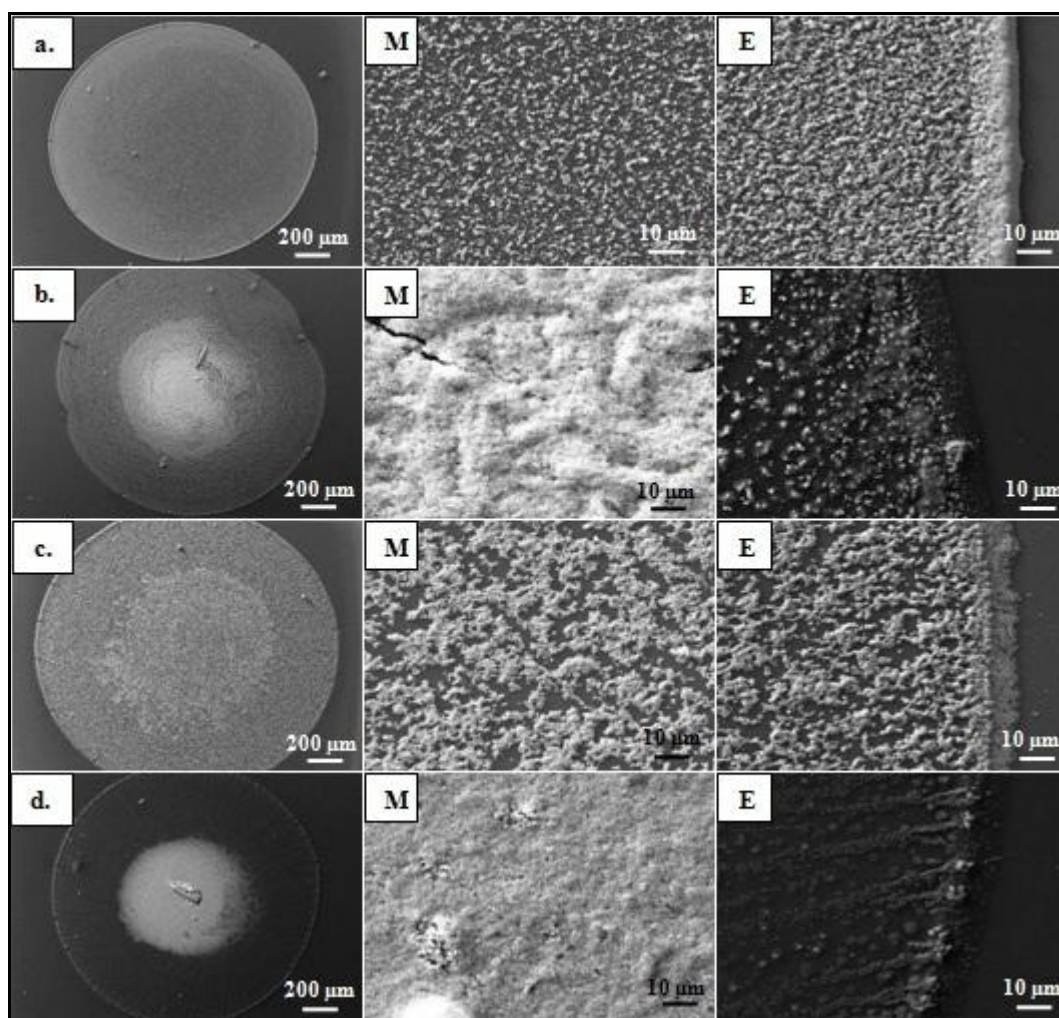


Figure 5.13. Comparison of SEM images of droplet areas of AgNP-protein containing droplets; a. Sessile: AgNP-HSA and c. AgNP-Cyt c, b. suspended: AgNP-HSA and d. AgNP-Cyt c (D). 'M' and 'E' denote middle and edge of the droplet area, respectively.

Images show a protein concentration of 50 $\mu\text{g/mL}$

The force of gravity, which is perpendicular to solvent flow, hinders a dense contact-line formation and accumulates AgNPs and proteins in the middle of the droplet area. The density of molecular species is higher in the middle of the droplet area than the density at the edges for both negatively and positively protein containing suspended dried droplets.

The packing density of nanoparticles through surface roughness for both sessile droplet and suspended droplet was investigated by AFM analysis. The AFM images were obtained from the edges of the sessile droplets and from the middle of the suspended dried droplets.

These regions were thought to be suitable for AFM analysis since they are the regions where the SERS spectra were collected. A negatively charged (HSA) and positively charged protein (Cyt c) were used for AFM analysis. The surface roughness of thin film-like structures composed of nanoparticles can be evaluated using an average roughness value (Ra) of the whole area from the AFM images. Figure 5.14.a and Figure 5.14.b show the AFM images obtained from the edge and middle region of a sessile and suspended dried droplet of AgNP-HSA, respectively. Figure 5.14.c and 5.14.d show the case for AgNP-Cyt c. Table 5.1 shows the average Ra values of obtained AFM images. The Ra values of suspended dried droplets for both HSA and Cyt c are greater than the Ra values of sessile dried droplets. The greater roughness indicates that the larger gap between AgNP-protein structures at the center of a suspended dried droplet area. This loose packing obviously has dramatic effect on the SERS performance of AgNPs through the efficient oscillation of the nanoparticle's electron system.

Figure 5.15 shows a comparison of the SERS spectra of HSA obtained from the middle region of a suspended dried droplet area, a thin film prepared with convective assembly [54], at the edge of a sessile dried droplet area, and AgNP aggregates themselves. The quality of the SERS spectra obtained from a suspended dried droplet is significantly better than the quality of the SERS spectra obtained from a sessile dried droplet. Due to the trapping of proteins between nanoparticles at the middle of the droplet, the interaction between AgNP clusters and proteins enhance significantly and even new Raman bands appear compared to the spectra obtained from protein-AgNP thin film prepared with convective assembly.

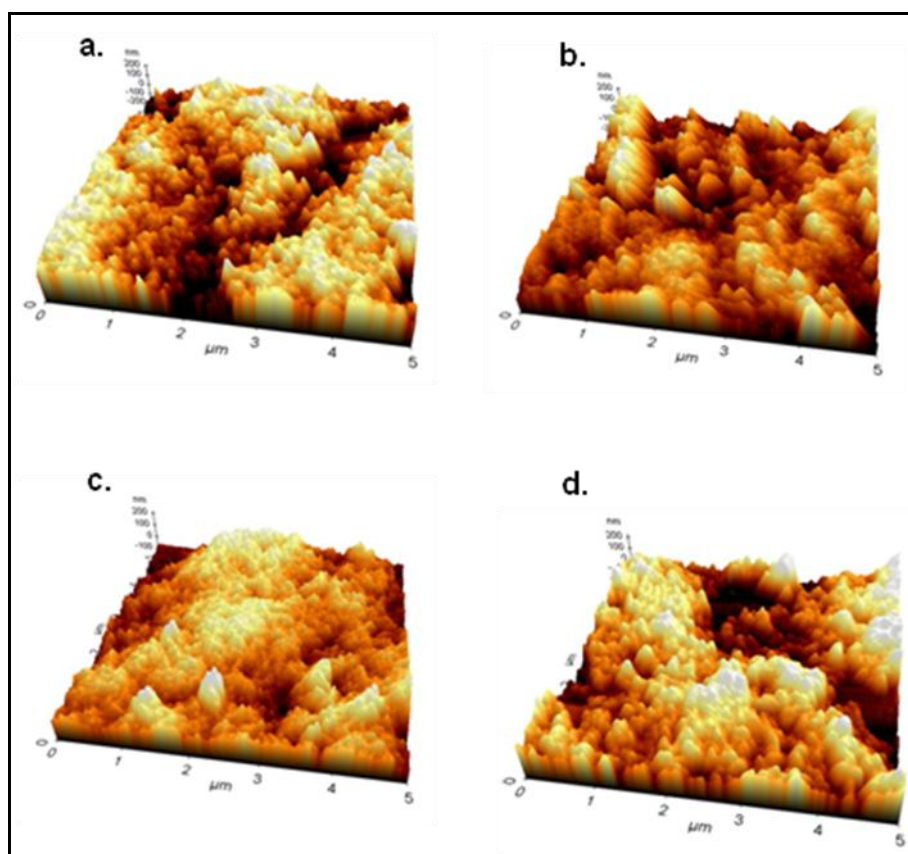


Figure 5.14. a. AFM images of HSA-AgNP containing sessile and b. suspended dried droplets and c. Cyt-c-AgNP containing sessile and d. suspended dried droplets. The images were obtained from the edges of sessile dried droplets and from the center of suspended dried droplets. The protein concentration of the experiment is 50 $\mu\text{g}/\text{mL}$

Table 5.1. Average Ra values of obtained AFM images

Droplet	Ra
HSA containing sessile dried droplet	3.695
HSA containing suspended dried droplet	14.698
Cyt c containing sessile dried droplet	25.536
Cyt c containing suspended dried droplet	38.028

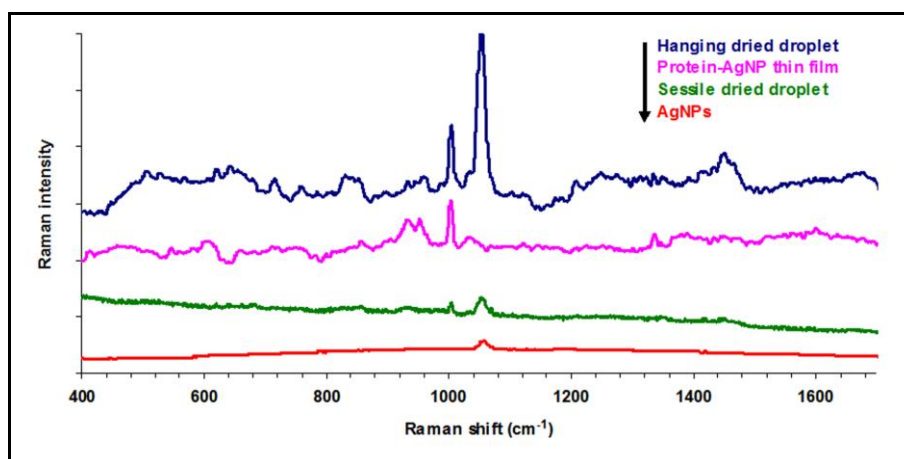


Figure 5.15. SERS spectra of an AgNP-HSA containing suspended dried droplet, a protein-AgNP thin film, a sessile droplet and silver colloidal suspension. The protein concentration of the experiment is 50 $\mu\text{g/mL}$

The reproducibility of the SERS spectra obtained from a suspended dried droplet was investigated by comparing ten SERS spectra which randomly collected from the dried droplet area. Figure 5.16 shows ten SERS spectra obtained from negatively and positively charged protein containing suspended dried droplets and white light images of the droplet area where these spectra were collected. The variations of the SERS spectra from different spots on the droplet area were calculated and the coefficient of variation values were found 16.0 per cent and 10.9 per cent for negatively and positively charged proteins, respectively. These values are satisfactory for comparison reasons [46, 70].

In conclusion, the SERS spectra obtained from different samples prepared by different sample preparation methods indicate that suspended droplet from a hydrophobic surface is the most suitable method over other approaches in the study and it was used in the following parts which involve determining the minimum detection limit of the selected proteins in AgNP suspension and investigating denaturation profiles of proteins with SERS.

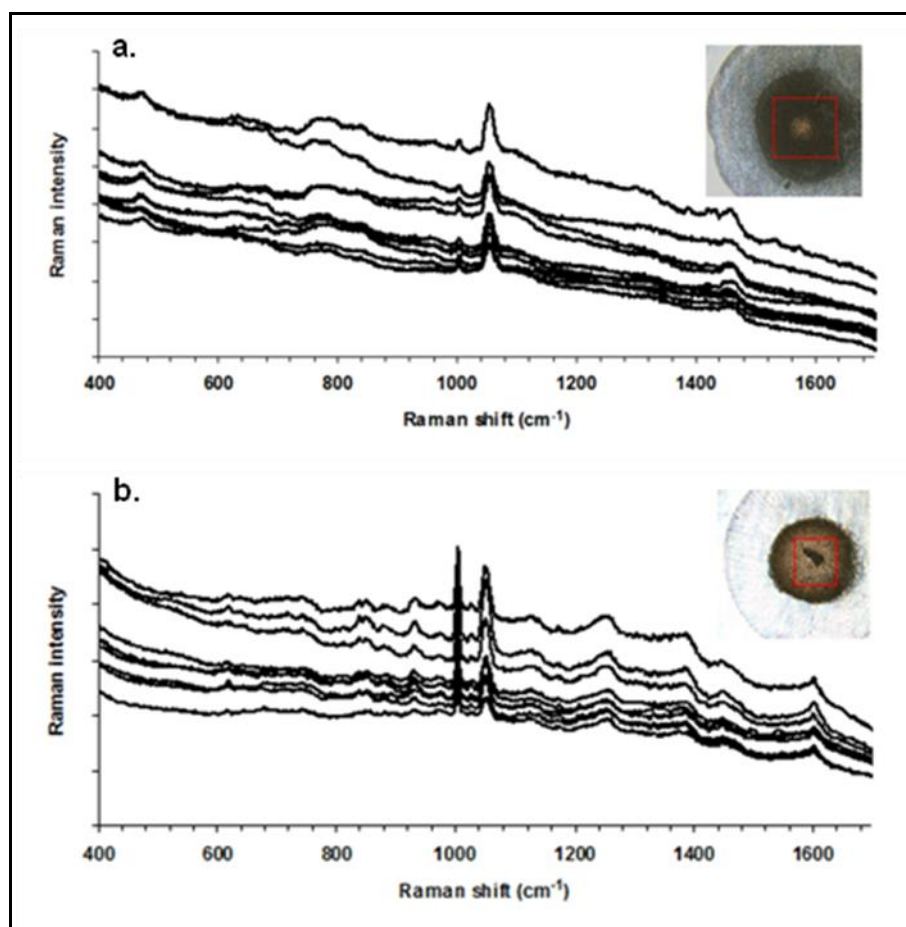


Figure 5.16. a. Ten SERS spectra obtained from negatively and b. positively charged protein containing suspended dried droplets and white light images of the droplet area where these spectra were collected. The protein concentration of the experiment is 50 $\mu\text{g/mL}$

5.1.3. Determining the Detection Limits of the Proteins

The minimum detection limit of three acidic (HSA, myoglobin, transferrin) and three basic proteins (avidin, Cyt c, lysozyme) was investigated. Figure 5.17 shows the SERS spectra of proteins with decreasing concentrations and Table 5.2 shows the band assignments of proteins. The SERS spectra of the proteins are consistent with the previously reported spectra in the literature [59, 63, 79, 94-96].

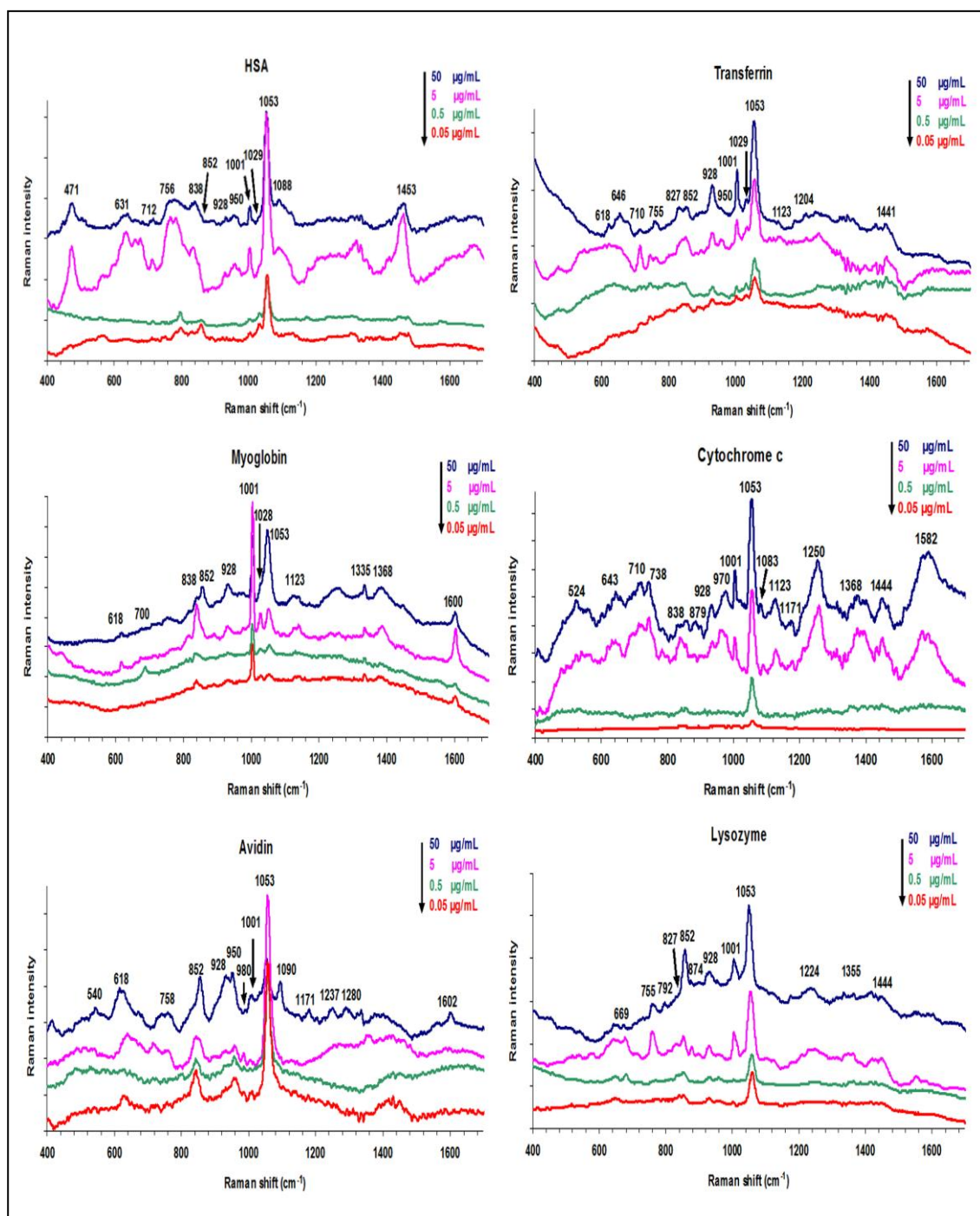


Figure 5.17. SERS spectra of HSA, transferrin, myoglobin, cytochrome c, avidin and lysozyme with their decreasing concentration in AgNP colloidal suspension

Table 5.2. Band assignments for SERS spectra of proteins

HSA	Transferrin	Myoglobin	Cyt c	Avidin	Lysozyme	Band Assignments
471	---	---	---	---	---	---
---	---	---	524	---	---	S-S str. ^[97]
---	---	---	---	540	---	Cys ^[98]
---	618	618	---	618	---	C-C twist. ^[99]
---	646	---	643	---	---	Tyr ^[100]
631	710	700	710	---	669	Met ^[99]
712			738			
756	755	---	---	758	755	Trp ^[60]
---	827	---	---	---	827	Pro, Tyr ^[100]
838	---	838	838	---	---	vibration of amine groups ^[101]
852	852	852	---	852	852	Tyr, Pro ^[98]
---	---	---	879	---	---	Trp, Pro ^[100]
928	928	928	928	928	928	Pro, Val ^[102]
950	950	---	---	950	950	Pro, Val ^[103]
---	---	---	970	---	---	Ser ^[60]
---	---	---	---	980	---	Trp ^[60]
1001	1001	1001	1001	1001	1001	Phe ^[60]
1029	1029	1028				
1053	1053	1053	1053	1053	1053	C-O, C-N str. ^[99]
1088	---	---	---	1090	---	C-C str. ^[104]
---	1123	1123	1083	---	---	C-N str. ^[97]
---			1123			
---	---	---	1171	1171	---	Try ^[60]
---	1204	---	---	---	---	Try+Phe ^[60]
---	---	---	---	---	1224	Amide III ^[105]
---	---	---	1250	---	---	Amide III ^[60]
---	---	---	---	1237	---	Gly, Pro ^[106]
---	---	---	---	1280		
---	---	1335	---	---	---	Trp ^[60]
---	---	1368	1368	---	1355	Trp ^[60]
---	1441	---	---	---	---	CH ₂ sciss. ^[60]
1453	---	---	---	---	---	Gly ^[60]
---	---	---	1444	---	1444	CH ₂ sciss. ^[60]
---	---	---	1582	---	---	Phe ^[60]
---	---	1600	---	1602	---	Amide I ^[106]

A detection limit down to 0.05 $\mu\text{g/mL}$ can be easily achieved by overturning the substrate the droplet located. We claim that the presented simple method significantly improves the spectral quality and reproducibility in a SERS experiment for all types of molecules and molecular structures.

5.1.4. Denaturation of Proteins with Heat and SERS Measurements

After determining the most appropriate method to obtain spectral acquisition in good quality, we used this simple approach (suspended droplet) to investigate the effect of protein denaturation on SERS spectra. It was mentioned that the hydrophobic residues of a protein mostly locate interior of its structure. When the protein reaches its melting point, it loses its three dimensional structure and hydrophobic residues such as phenylalanine, tyrosine, tryptophan which give good SERS signal, come to contact with or close vicinity to metallic nanoparticles. There are many reports, which indicate the positive effect of high temperature on SERS performance, in the literature [107-109]. Also, it was shown that minor changes occurring in protein structure between a temperature range of -90 and 90 $^{\circ}\text{C}$ can be observed with SERS [95].

Four acidic and two basic proteins were used in the heating experiments. The proteins in different mixtures were selected based on the charge they possess. Since the charge of the analyte influences dramatically the distribution of AgNPs and analyte molecules on the droplet area. In binary mixtures, three different combinations (negative-negative, positive-positive and negative-positive) were used.

The approximate melting points of the proteins were investigated by using DLS. The method involves the increasing temperature of protein solution and determining the size distribution of the particles at each temperature. When the protein reaches its melting point, the structure of the protein unfolds and this is observed as logarithmic curve on the graph of size versus temperature as seen on Figure 5.18. Table 5.3 shows the approximate melting point values of the proteins in the study.

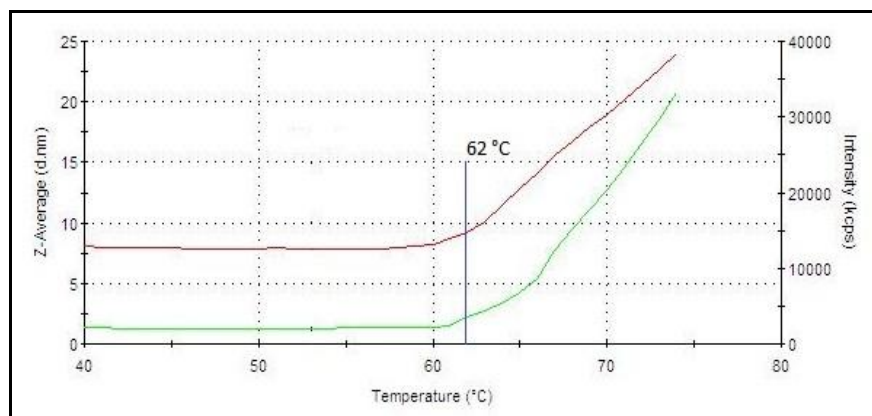


Figure 5.18. Graph of size versus temperature for HSA

Table 5.3. Melting point values of the proteins in the study

Protein	Melting Point (°C)
HSA	62
Transferrin	68
Myoglobin	42
Hemoglobin	42
Cyt c	66
Lysozyme	68

When a droplet of a mixture of a protein and colloidal AgNPs is heated during the SERS spectral acquisition, the conformational changes in the protein structure are reflected on the spectra. At around the melting temperature of the protein, a dramatic change in the spectra is expected. This change in the pattern of the SERS spectra can be used to detect and identify different proteins in a multiple protein mixture.

Figure 5.19 shows the SERS spectra of single proteins at different temperatures. As seen, the intensity of the band 676 cm^{-1} , which is associated with methionine [97], increases as the temperatures increases. Met has hydrophobic side-chains and locates interior of the protein structure. When the compact structure of transferrin opens at high temperature, met residues buried in the protein are possibly come in contact with the AgNP surfaces and this is reflected to the SERS spectra.

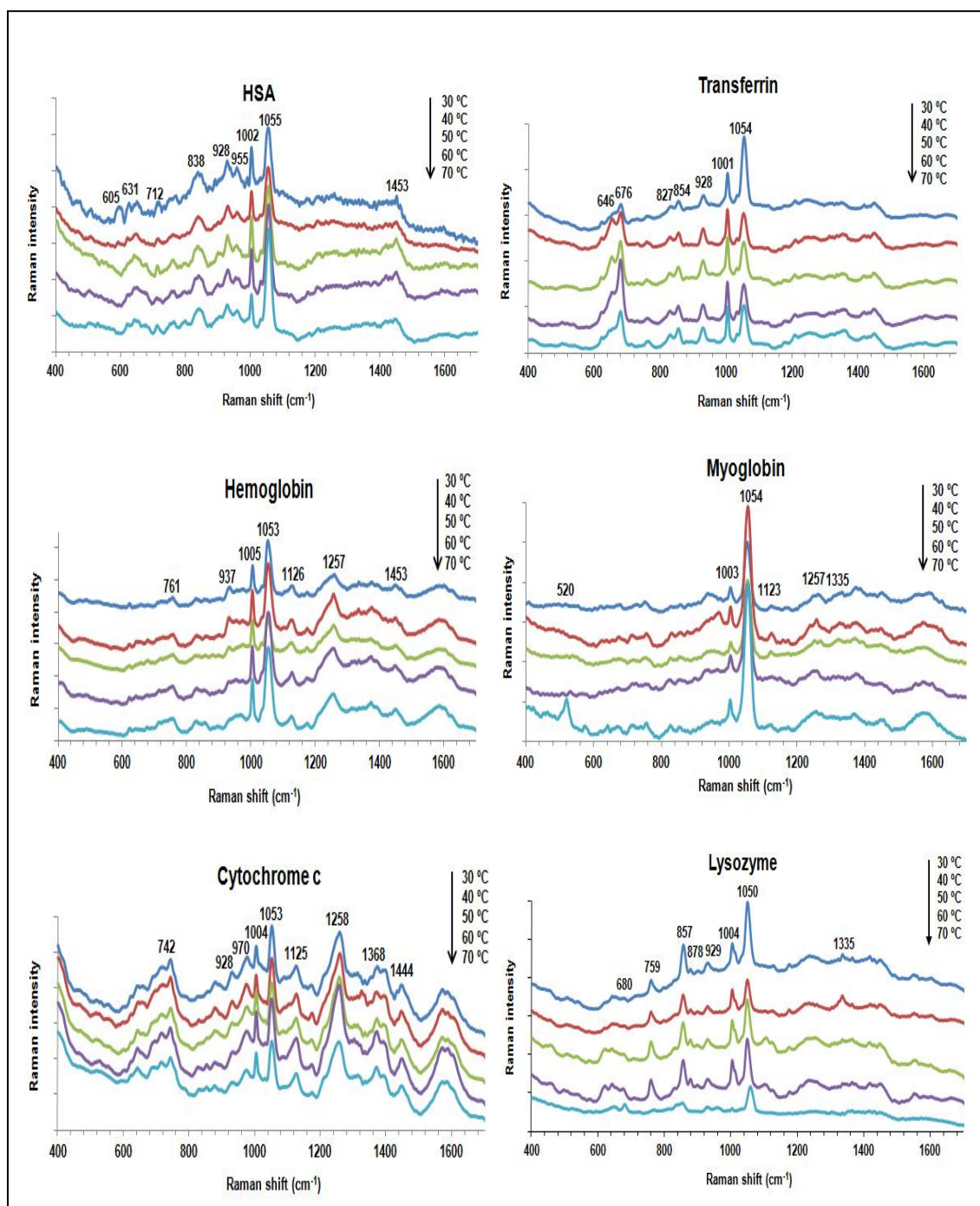


Figure 5.19. SERS spectra of single proteins in the study at different temperatures

The differences in the SERS spectra at different temperatures cannot be identified visually in some cases. In order to observe the spectral changes in a clear manner, a statistical program, SPSS (originally, Statistical Package for the Social Sciences), was used. In Multi-dimensional scaling of SPSS, each spectrum can be reduced into one spot on a 2D or 3D

coordinate system using Euclidean Distances. The most straightforward and generally accepted way of computing distances between objects in a multi-dimensional space is to compute Euclidean distances, an extension of Pythagoras' theorem. It measures the distances between objects based on a clustering algorithm. The clustering algorithm determines the rules that govern between which points distances are measured to determine cluster membership. In the algorithm, we used the cluster membership assessment by calculating the total sum of deviations from the mean of a cluster. The closeness of the coordinates indicates the close relationship among the spectra. In this study, the 2D plots were used for the data presentation. Every spot on each 2D plot is associated to the average of five SERS spectra.

5.1.4.1. SERS Measurements of Binary Protein mixtures with AgNPs

Figure 5.20.a and 5.20.b show the SERS spectra of mixture of HSA and transferrin, which are both negatively charged proteins, with AgNPs at increasing temperatures and 2D Euclidean Distance plot, respectively. The numbers next to the spots on the plots refer to the temperature of the sample when the SERS spectra were collected. As seen in Figure 5.20.a, Raman bands at 676, 827 and 855 cm^{-1} belong to transferrin. As seen in Figure 5.20.b, the 2D plot indicates that there is a very obvious similarity between the spectra of transferrin and mixture at 30 °C, since their spots are very close to each other. When the temperature increases, the resemblance between the spectra of the mixture and transferrin decreases and the SERS spectra of the mixture show a similarity to the spectra of HSA, particularly at 70 °C due to the increasing of the band at 955 cm^{-1} which is associated with HSA.

A similar phenomenon was observed in the case of HSA and myoglobin mixture (the proteins are both negatively charged). Figure 5.21.a and 5.21.b show the SERS spectra of HSA, Mb and AgNPs mixture at increasing temperatures and 2D Euclidean Distance plot. The intensity of the band at 1257 cm^{-1} , which is associated with Mb, decreases at 60-70 °C. The same case was observed in the mixture of single Mb and AgNP. In addition, the intensity of the band at 760 cm^{-1} , which is also associated with Mb, starts to increase at 40 °C. The 2D plot indicates that the SERS spectra of the mixture are similar to the spectra of myoglobin at 70 °C.

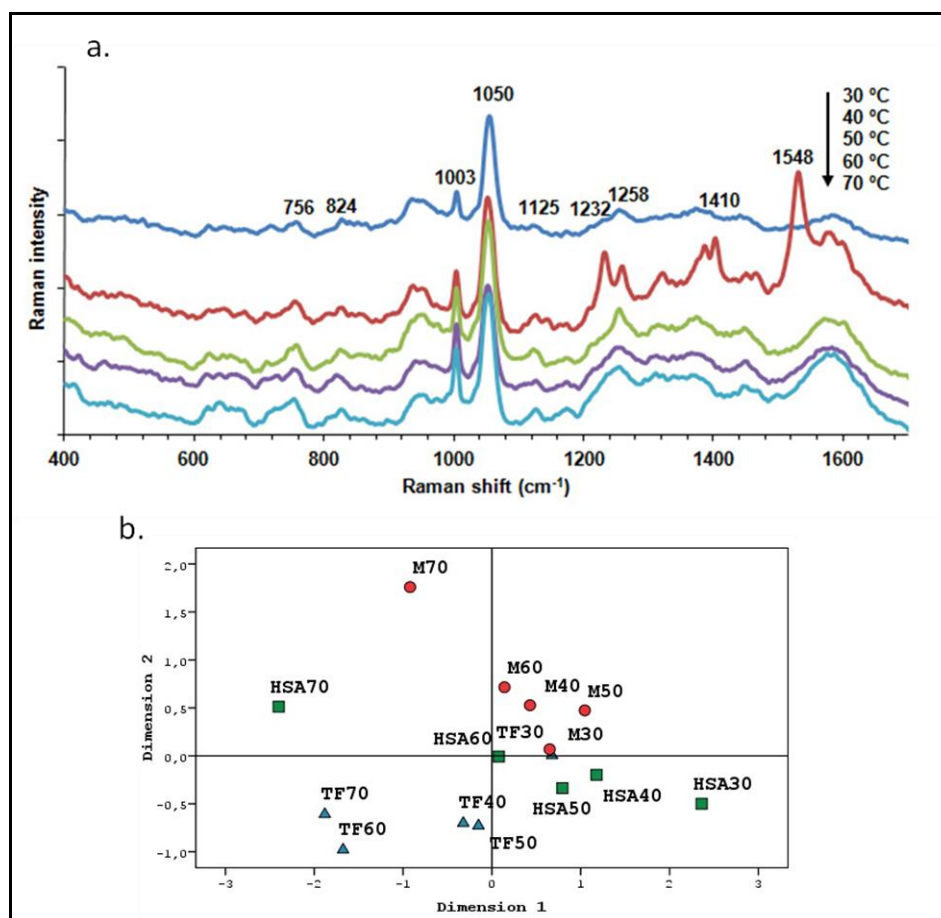


Figure 5.20. a. SERS spectra of HSA, Transferrin and AgNP mixture at increasing temperatures and b. 2D Euclidean Distance plot, TF: Transferrin, HSA: Human Serum Albumin, M: Mixture

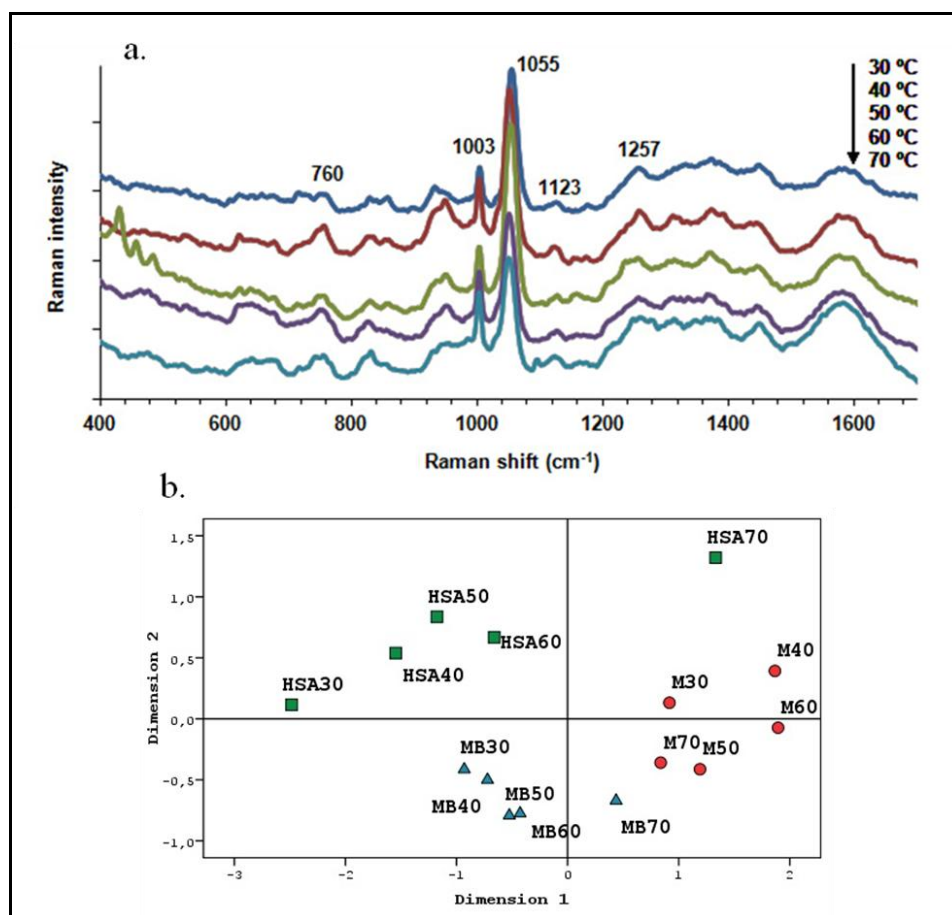


Figure 5.21. a. SERS spectra of HSA, Mb and AgNP mixture at increasing temperatures and b. 2D Euclidean Distance plot, MB: Myoglobin, HSA: Human Serum Albumin, M: Mixture

Figure 5.22.a and Figure 5.22.b show the SERS spectra of two positively charged proteins, Cyt c and lysozyme, with AgNPs, 2D Euclidean Distance plot. As seen in Figure 5.22.a, the band of 1444 cm^{-1} belongs to Cyt c and the bands at 758 and 882 cm^{-1} belong to lysozyme. The intensity of the bands at 758 and 882 cm^{-1} decreases when the temperature increases to $70\text{ }^{\circ}\text{C}$. This case was also observed in the mixture of single lysozyme and AgNP. Additionally, the 2D plot, which is on Figure 5.22.b, supports this hypothesis. As seen, the spectra of the mixture and lysozyme locate on similar coordinates on the plot. On the other hand, the most of the peaks, which were observed in the mixture of single Cyt c and AgNP, could not be observed in the mixture of Cyt, lysozyme and AgNP. According to best of our knowledge, this case is a result of greater size and positive charge of

lysozyme over Cyt c. Therefore, lysozyme can interact with AgNPs more effectively compared to the interaction between Cyt c and AgNPs.

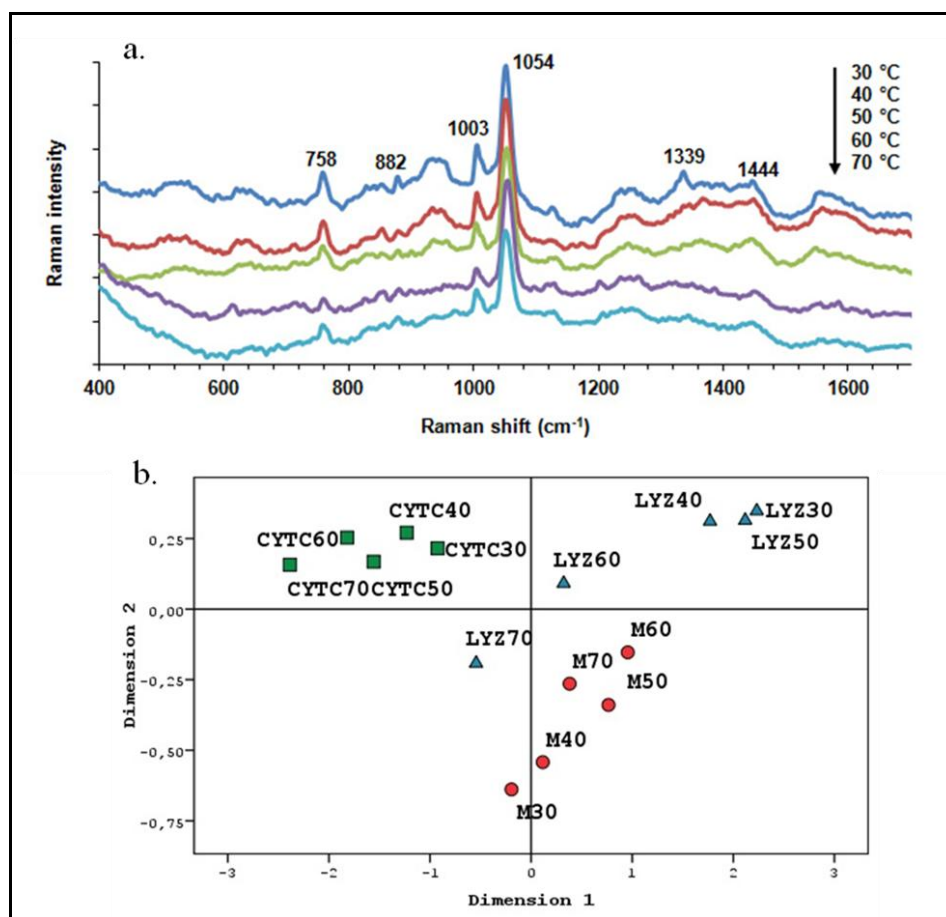


Figure 5.22 .a SERS spectra of Cyt c, lysozyme and AgNP mixture at increasing temperatures and b. 2D Euclidean Distance plot (B), CYTC: Cytochrome c, LYZ: Lysozyme, M: Mixture

Figure 5.23.a and Figure 5.23.b show the SERS spectra of a mixture that contains one positively (lysozyme) and one negatively (hemoglobin) charged protein with AgNPs and 2D Euclidean Distance plot. The band at 675 cm^{-1} is associated with only lysozyme and the band at 765 cm^{-1} is associated with both of the proteins in the mixture. As seen in Figure 5.32.b, the spectra of the mixture and lysozyme show a similarity to each other at 40 and 50 °C. The 2D plot gives an outcome as it was expected, since it is obvious that lysozyme can interact with negatively charged AgNP more effectively and dominate the spectra of the mixture due to its positive charge.

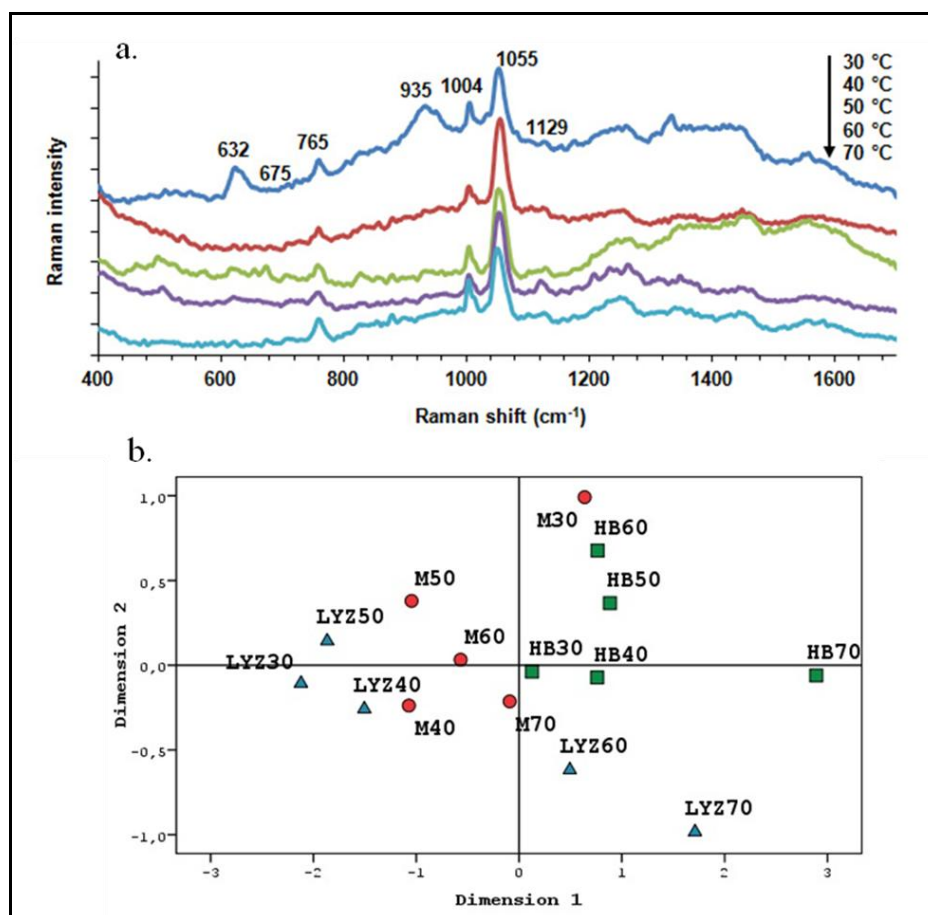


Figure 5.23. a. SERS spectra of Hb, lysozyme and AgNP mixture at increasing temperatures and b. 2D Euclidean Distance plot, HB: Hemoglobin, LYZ: Lysozyme, M: Mixture

5.1.4.2. SERS Measurements of Ternary Protein Mixtures with AgNPs

Figure 5.24.a to Figure 5.24.f show the SERS spectra of the mixture of HSA, Tf and Mb with AgNPs (they are all negatively charged proteins) at increasing temperatures and 2D Euclidean Distances plots for each temperature (b: 30 °C; c: 40 °C; d: 50 °C; e: 60 °C; f: 70 °C). We have preferred to analyze the spectra of mixtures at individual temperatures to simplify the comparison.

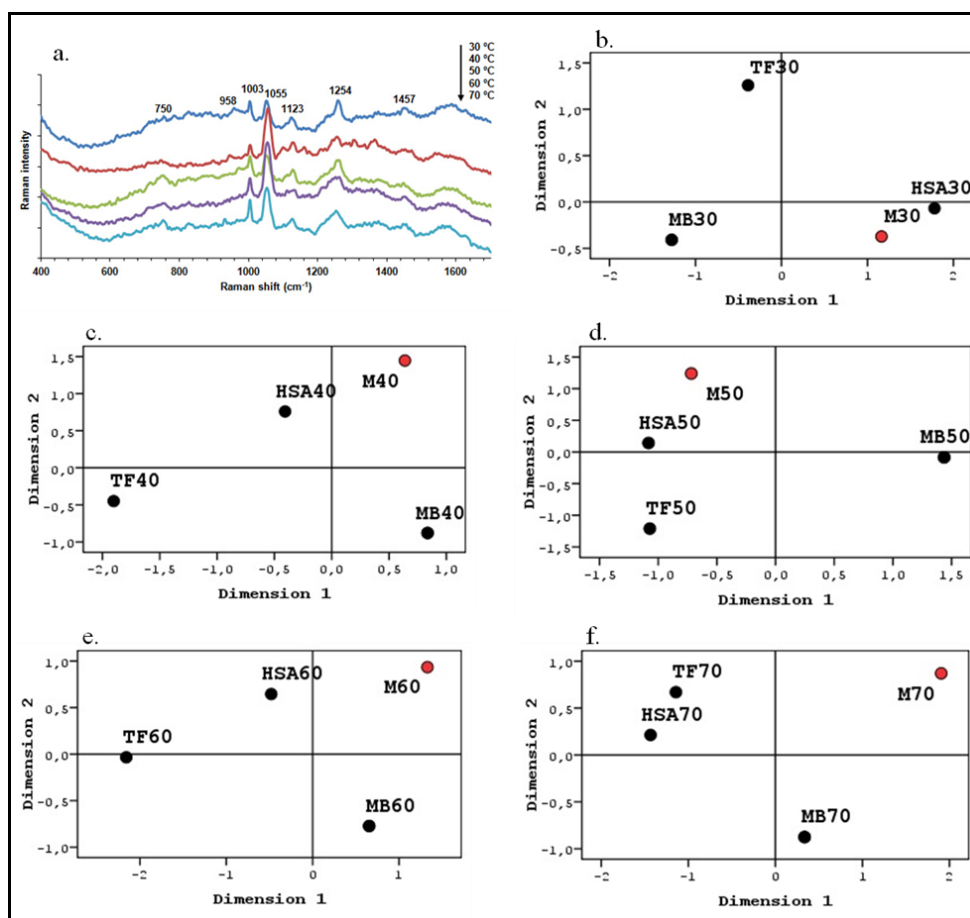


Figure 5.24.a. SERS spectra of the mixture of HSA, Tf and Mb with AgNPs at increasing temperatures and 2D Euclidean Distance plots (b: 30 °C; c: 40 °C; d: 50 °C; e: 60 °C; f: 70 °C)

As seen in Figure 5.24.a, the bands at 1123 and 1254 cm⁻¹ are associated with Mb molecules in the mixture and the bands at 958 and 1457 cm⁻¹ are associated with Tf molecules. The 2D plots indicate that the spectra of HSA dominate the spectra of the mixture at almost all temperatures due to the possible high affinity of AgNPs to HSA proteins. This affinity could be the result of high ratio of Cys amino acids in HSA structure and comparably great hydrodynamic radius of HSA which also positively affects the interparticle distance in AgNP aggregates [104].

Figure 5.24.a to Figure 5.24.f show the SERS spectra of the mixture of negatively charged proteins, HSA, Transferrin and Hb, at increasing temperatures and 2D Euclidean Distances plots for each temperature (b: 30 °C; c: 40 °C; d: 50 °C; e: 60 °C; f: 70 °C).

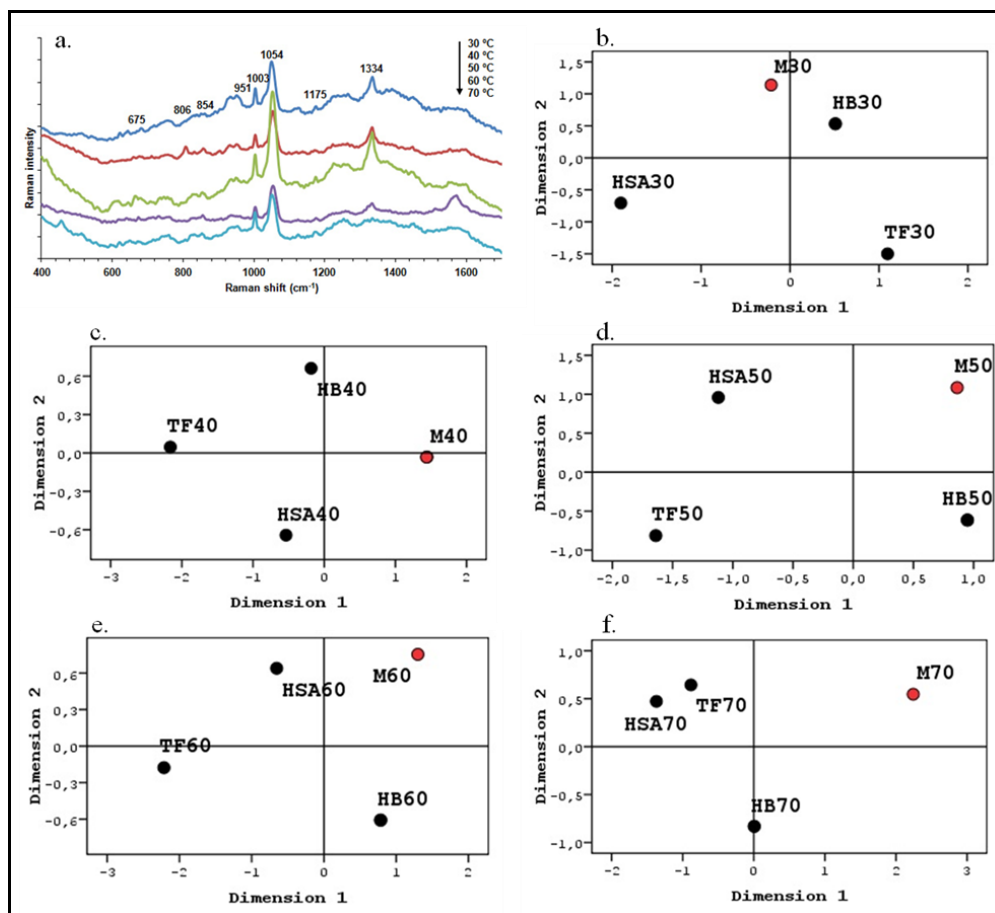


Figure 5.25.a. SERS spectra of the mixture of HSA, Tf and Hb with AgNPs at increasing temperatures and 2D Euclidean Distance plots for each temperature (b: 30 °C; c: 40 °C; d: 50 °C; e: 60 °C; f: 70 °C)

As seen in Figure 4.25.a, the peaks at 675 and 854 cm^{-1} are associated with Tf. The peak at 1334 cm^{-1} , which was not observed in the individual spectra of proteins, is highly intense in the spectra of the mixture. This intense pick is associated with CH_3CH_2 deformation and indicates that the proteins do not interact with only AgNP, but also with each other. Therefore, it causes to appear new Raman bands. 2D coordinate systems show that the spectra of the mixture show a similarity to Hb at 30, 40 and 50 °C since these temperature values are close to the melting point of Hb. When the temperature reaches 60 °C, the spectra of the mixture start to resemble more HSA and when it is 70 °C, the spots that belong to each protein locate on far coordinates from the spot of the mixture on 2D plot. The reason of this case is probably that all proteins in the mixture open their structure at 70

°C and start to interact with AgNPs more effectively, even though it was not reflected on the spectra at 70 °C.

Figure 5.26.a to Figure 5.26.f show the SERS spectra of a mixture that contains two negatively charged (HSA and transferrin) and one positively charged (Cyt c) protein (A) and 2D Euclidean Distance plots for each temperature (b: 30 °C; c: 40 °C; d: 50 °C; e: 60 °C; f: 70 °C). As seen in Figure 5.26.a, all of the obtained peaks were also obtained from single Cyt c and AgNP mixture. Cyt c is the only positively charged protein in the mixture and its molecular weight is 3-5 times less than the molecular weights of the proteins in the mixture. Therefore, the amount of Cyt c molecules is 3-5 times greater than the amount of other protein molecules in the mixture since they are all in same concentration. Due to its high amount and positive charge, Cyt c dominates the spectra of the mixture as it is expected and seen on 2D plots.

Figure 5.27.a and 5.27.f show the SERS spectra of a mixture that contains two negatively charged (Hb and transferrin) and one positively charged (Cyt c) protein and 2D Euclidean Distance plots for each temperature (b: 30 °C; c: 40 °C; d: 50 °C; e: 60 °C; f: 70 °C). In Figure 5.27.a, 760 cm^{-1} band is associated with Hb and 1125, 1258 and 1446 cm^{-1} bands are associated with both Tf and Cyt c. Hb is a oxygen-binding metalloprotein, which has a electron-rich porphyrin group that gives good SERS signal. The melting point of Hb was found 42 °C and lower than other proteins in the mixture. Therefore, its structure opens first and keeps dominating the spectra of the mixture until 60 °C and when the temperature reaches 70 °C, all proteins in the mixture start to interact with NPs effectively.

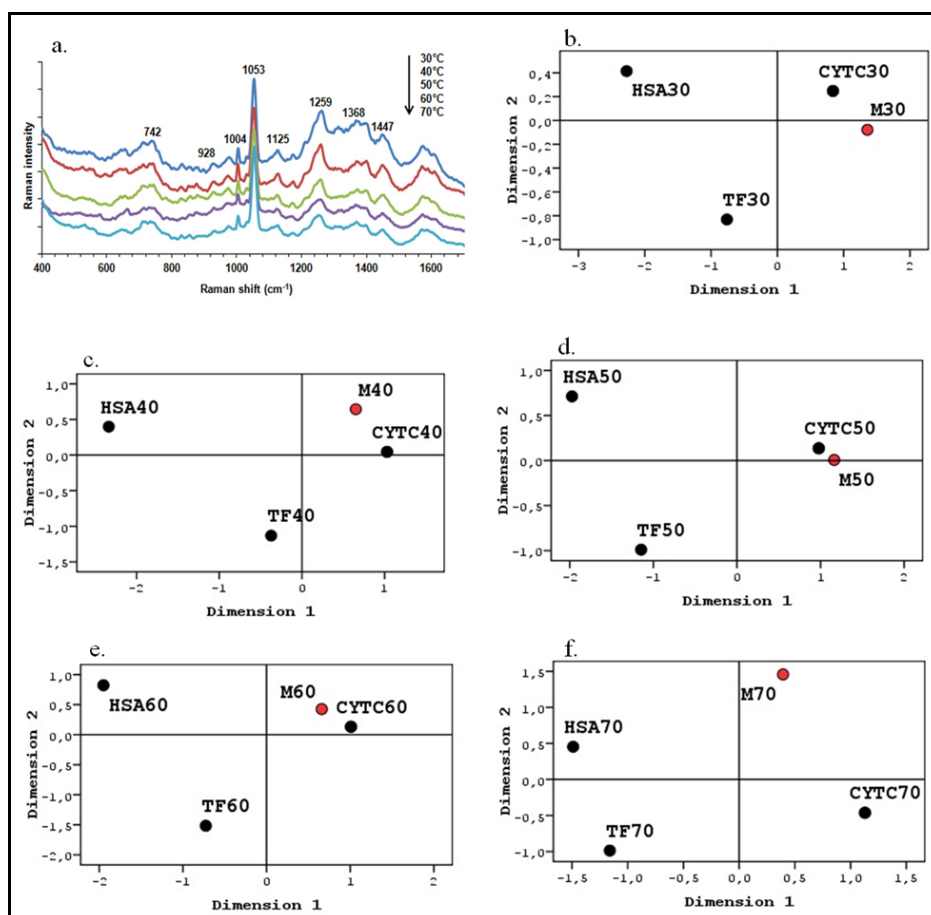


Figure 5.26. a. SERS spectra of the mixture of HSA, Transferrin and Cyt c with AgNPs at increasing temperatures and 2D Euclidean Distance plots for each temperature (b: 30 °C; c: 40 °C; d: 50 °C; e: 60 °C; f: 70 °C)

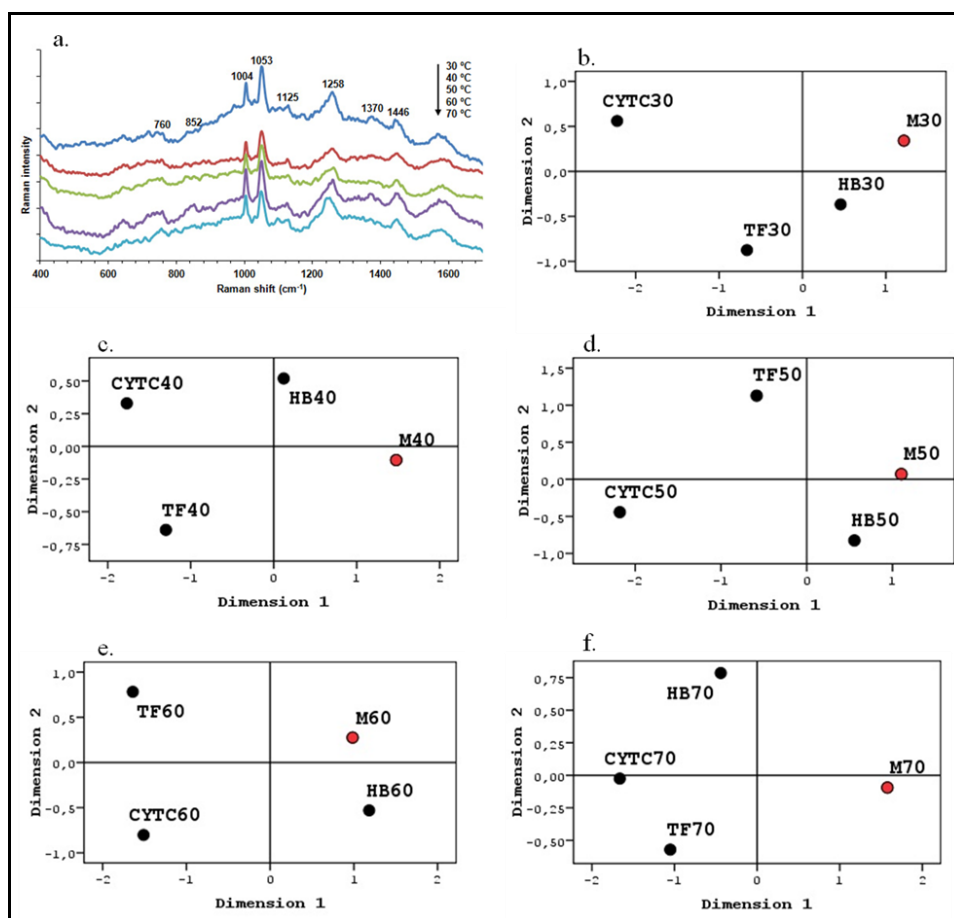


Figure 5.27.a. SERS spectra of the mixture of Hb, Transferrin and Cyt c with AgNPs at increasing temperatures and 2D Euclidean Distance plots for each temperature (b: 30 °C; c: 40 °C; d: 50 °C; e: 60 °C; f: 70 °C)

The data obtained from binary and ternary protein mixtures indicates that this method is promising for label-free protein detection from multiple protein mixtures with SERS. The distribution of the spots, which refer to SERS spectra of different proteins, on 2D Euclidean Distance plot can be used to generate a database for protein identification from multiple protein mixtures. The localization of the spots of mixtures and individual proteins gives valuable information about the behaviors of the proteins in different combinations of multiple protein mixtures.

6. CONCLUSION AND RECOMMENDATIONS

6.1. CONCLUSION

In this study, we demonstrated two simple and effective approaches for the manipulation of nanoparticles and molecular species in drying droplets, which can be used for obtaining reproducible and rich SERS spectra. The first approach involves dipping a tip into a drying droplet and an improvement in detection limit of negatively charged proteins more than one order of magnitude was achieved. The detection limit for BSA is at the picomolar level. However, no significant improvement was observed with positively charged Cyt c. Dipping a tip into a droplet on a surface is a very simple procedure. However, the benefit from this simple procedure is incredible. The second approach involves hanging the droplet against gravity during drying. In this method, the accumulation of proteins and AgNPs in the middle of the droplet occurs regardless of the protein surface charge, shape and size, under the influence the force of gravity compared to the sessile dried droplet. A detection limit of 0.05 $\mu\text{g/mL}$ can be easily achieved with this method. The results indicate that the quality and reproducibility of the SERS spectra from anywhere in the middle of the droplet area is satisfactory for comparison. The presented simple method significantly improves the SERS spectral quality and reproducibility for proteins and we claim that suspended-droplet method can be applied to all types of molecules and molecular structures.

The improved sample preparation method, which involves suspending droplet from a hydrophobic surface, was used to investigate the conformational changes of proteins at increasing temperatures with using SERS. The combination of the SERS spectra obtained at increasing temperatures and a clustering algorithm allows identification of proteins in a multiple mixture. We claim that this is a promising method to generate a database for protein detection and identification. After SERS acquisition of a protein mixture whose protein content is unknown, the SERS spectra can be processed by a statistical program and it matches with a distribution pattern of spots on a two or three dimensional space recorded in the database. However, generating such a database requires repeating experiments with different batches of AgNP suspensions for at least three times. Further

analysis to prove the reliability of the method will be done and it will be the second step of the presented study.

6.2. RECOMMENDATIONS

The sample preparation method of suspending a droplet from a hydrophobic surface can be used to detect various kinds of biological molecules such as DNA, RNA, bacteria or viruses with the use of SERS. This method provides a very simple and effective way to manipulate the localization of particles and any molecular species in a drying droplet. Therefore, it can be a promising candidate to assemble nanostructures on a certain area based on evaporation-mediated assembly.

Generating a database based on the spectral differences of proteins with the assistance of a statistical program has a great potential to identify the proteins in a multiple protein mixture. Combination of the software of Raman microscopy and a statistical program can decrease the duration of the process and also provides more simplicity and reliability to detect various types of molecular structures.

Heating protein mixtures in an aqueous suspension rather than a dried droplet and obtaining SERS acquisition simultaneously may provide more significant information about the thermodynamic events occurring in protein structure as temperature increases. Since, the proteins behave more freely and are more sensitive to temperature changes in solution, studying the temperature versus SERS may provide more information in solution. A separation step can also be added into the current procedure in order to further increase the applicability of the technique for real samples. It was shown that convective assembly could be used to separate proteins. Therefore, separation of protein mixtures on a hydrophilic surface with convective assembly can be a good candidate for the purpose.

REFERENCES

1. Daniel, M. C. and Astruc, D., “Gold nanoparticles: Assembly, supramolecular chemistry, quantum-size-related properties, and applications toward biology, catalysis, and nanotechnology”, *Chem. Rev.*, Vol. 104, No. 1, pp. 293-346, 2004.
2. Faraday, M. Experimental Relations of Gold (and other Metals) to Light. *Philos. Trans.*, Vol. 147, pp. 145-181, 1857.
3. Feynman, R. P., There’s Plenty of Room at the Bottom, <http://www.its.caltech.edu/~feynman/plenty.html>, 1959, [retrieved 8 January 2012].
4. Taniguchi N., On the basic concept of 'Nano-Technology'. *Proc. Intl. Conf. Prod. London, Part II, British Society of Precision Engineering*, 1974.
5. Wolf, E. L., *Nanophysics and Nanotechnology: An Introduction to Modern Concepts in Nanoscience*, Wiley-VCH, Weinheim, 2004.
6. Bange, A., Halsall, H.B. and Heineman, W.R., “Microfluidic immunosensor systems” *Biosensors & Bioelectronics*, Vol. 20, No. 12, pp. 2488-2503, 2005.
7. Li, J. N., Zhang, Z., Rosenzweig, J., Wang, Y. Y., Chan, D. W., “Proteomics and bioinformatics approaches for identification of serum biomarkers to detect breast cancer”, *Clin. Chem.*, Vol. 48, No. 8, pp. 1296–1304, 2002.
8. Baggerly, K. A., Morris, J. S., Coombes, K. R., “Reproducibility of SELDI-TOF protein patterns in serum: Comparing datasets from different experiments”, *Bioinformatics*, Vol. 20, No. 5, pp. 777–785, 2004.
9. Templin, M.F., Stoll, D. and Schrenk, M., “Protein microarray technology” *Trends In Biotechnology*, Vol. 20, No. 4, pp. 160-166, 2002.

10. Murphy, G.P., Elgamal, A.-A.A., Su, S.L., Bostwick, D.G., Holmes, E.H., “Current evaluation of the tissue localization and diagnostic utility of prostate specific membrane antigen” *Cancer*, Vol. 83, No. 11, pp. 2259–2269, 1998.
11. Kumar, R., “A real-time immuno-PCR assay for the detection of transgenic Cry1Ab protein”, *European Food Research and Technology*, Vol. 234, No. 1, pp. 101-108, 2012.
12. Yoshida, Y., Horii, K., Sakai, N., Masuda, H., Furuichi, M., Waga, I., “Antibody-specific aptamer-based PCR analysis for sensitive protein detection”, *Analytical and Bioanalytical Chemistry*, Vol. 395, No. 4, pp. 1089-1096, 2009.
13. Gramotnev, D. K., Bozhevolnyi, S. I., “Plasmonics beyond the diffraction limit”, *Nat. Photonics*, Vol. 4, No. 2, pp. 83-91, 2010.
14. Schuller, J. A., Barnard, E. S., Cai, W., Jun, Y. C., White, J. S., Brongersma, M. L., “Plasmonics for extreme light concentration and manipulation”, *Nat. Mater.*, Vol. 9, No. 3, pp. 193-204, 2010.
15. Lal, S., Link, S., Halas, N. J., “Nano-optics from sensing to waveguiding”, *Nat. Photonics*, Vol. 1, No. 11, pp. 641-648, 2007.
16. Hutter, E., Fendler, J. H., “Exploitation of localized surface plasmon resonance”, *Adv. Mater.*, Vol. 16, No. 19, pp. 1685-1706, 2004.
17. Haes, A. J., Van Duyne, R. P., “A unified view of propagating and localized surface plasmon resonance biosensors”, *Anal. Bioanal. Chem.*, Vol. 379, No. 7-8, pp. 920-930, 2004.
18. Rycenga, M., Cobley, C.M., Zeng, J., Li, W., Moran, C.H., Zhang, Q., Qin, D., Xia, Y., “Controlling the Synthesis and Assembly of Silver Nanostructures for Plasmonic Applications”, *Chemical Reviews*, Vol. 111, No. 6, pp. 3669-3712, 2011.

19. Schatz, G.C. and Van Duyne, R.P. in *Handbook of Vibrational Spectroscopy*, Vol. 1, Wiley, New York, 2002.
20. Brockman, J.M., Nelson, B.P. and Corn, R.M., “Surface plasmon resonance imaging measurements of ultrathin organic films”, *Ann. Rev. Phys. Chem.*, Vol. 51, pp. 41-66, 2000.
21. Srituravanich, W., Fang, N., Sun, C., Luo, Q., and Zhang, X., “Plasmonic nanolithography”, *Nano Lett.*, Vol. 4, No. 6, pp. 1085-1088, 2004.
22. Bohren, C. F., Huffman, D. R., “Absorption Cross-Section Maxima and Minima in IR Absorption Bands of Small Ionic Ellipsoidal Particles”, *Applied Optics*, Vol. 20, No. 6, pp. 959-962, 1983.
23. Reinhard, B., Sheikholeslami, S., Mastroianni, A., Alivisatos, A. P., Liphardt, J., “Use of Plasmon Coupling to Reveal the Dynamics of DNA Bending and Cleavage by Single EcoRV Restriction Enzymes”, *Proc. Natl. Acad. Sci. U.S.A.*, Vol. 104, No. 8, pp. 2667–2672, 2007.
24. Sönnichsen, C., Reinhard, B. M., Liphardt, J., Alivisatos, A. P., “A Molecular Ruler Based on Plasmon Coupling of Single Gold and Silver Nanoparticles”, *Nat. Biotechnol.*, Vol. 23, No. 6, pp. 741–745, 2005.
25. Elghanian, R., Storhoff, J. J., Mucic, R. C., Letsinger, R. L., Mirkin, C. A., “Selective Colorimetric Detection of Polynucleotides Based on the Distance-Dependent Optical Properties of Gold Nanoparticles”, *Science*, Vol. 277, No. 5329, pp. 1078–1080, 1997.
26. Haes, A. J., Van Duyne, R. P., “A Nanoscale Optical Biosensor: Sensitivity and Selectivity of an Approach Based on the Localized Surface Plasmon Resonance Spectroscopy of Triangular Silver Nanoparticles”, *J. Am. Chem. Soc.*, Vol. 124, No. 35, pp. 10596–10604, 2002.

27. Sokolov, K., Follen, M., Aaron, J., Pavlova, I., Malpica, A., Lotan, R., Richards-Kortum, R., “Real-Time Vital Optical Imaging of Precancer Using Anti-Epidermal Growth Factor Receptor Antibodies Conjugated to Gold Nanoparticles”, *Cancer Res.*, Vol. 63, No. 9, pp. 1999–2004, 2003.
28. El-Sayed, I. H., Huang, X., El-Sayed, M. A., “Surface Plasmon Resonance Scattering and Absorption of Anti-EGFR Antibody Conjugated Gold Nanoparticles in Cancer Diagnostics: Applications in Oral Cancer”, *Nano Lett.*, Vol. 5, No. 5, pp. 829–834, 2005.
29. Alivisatos, A. P., “The Use of Nanocrystals in Biological Detection”, *Nat. Biotechnol.*, Vol. 22, No. 1, pp. 47–52, 2004.
30. Rosi, N. L., Mirkin, C. A., “Nanostructures in Biodiagnostics”, *Chem. Rev.*, Vol. 105, No. 4, pp. 1547–1562, 2005.
31. Hirsch, L. R., Stafford, R. J., Bankson, J. A., Sershen, S. R., Rivera, B., Price, R. E., Hazle, J. D., Halas, N. J., West, J. L., “Nanoshell-Assisted Tumor Ablation Using near Infrared Light under Magnetic Resonance Guidance” *Proc. Natl. Acad. Sci. U.S.A.*, Vol. 100, No.23, pp. 13549–13554, 2003.
32. Huang, X., El-Sayed, I. H., Qian, W., El-Sayed, M. A., “Cancer Cell Imaging and Photothermal Therapy in the Near-Infrared Region by Using Gold Nanorods”, *J. Am. Chem. Soc.*, Vol. No. 6, 128, pp. 2115–2120, 2006.
33. El-Sayed, I. H., Huang, X., El-Sayed, M. A., “Selective Laser Photo-Thermal Therapy of Epithelial Carcinoma Using Anti-EGFR Antibody Conjugated Gold Nanoparticles”, *Cancer Lett.*, Vol. 239, No. 1, pp. 129–135, 2006.
34. O’Neal, D. P., Hirsch, L. R., Halas, N. J., Payne, J. D., West, J. L., “Photo-thermal Tumor Ablation in Mice Using near Infrared-Absorbing Nanoparticles”, *Cancer Lett.*, Vol. 209, pp. No. 2, 171–176, 2004.

35. Loo, C. A., Lowery, A., Halas, N., West, J., Drezek, R., “Immunotargeted Nanoshells for Integrated Cancer Imaging and Therapy”, *Nano Lett.*, Vol. 5, No. 4, pp. 709–711, 2005.
36. Jain, P. K., El-Sayed, I. H., El-Sayed, M. A., “Au Nanoparticles Target Cancer”, *Nano Today*, Vol. 2, No. 1, pp. 18–29, 2007.
37. Huang, X., Jain, P. K., El-Sayed, I. H., El-Sayed, M. A., “Gold Nanoparticles: Interesting Optical Properties and Recent Applications in Cancer Diagnostics and Therapy”, *Nanomedicine*, Vol. 2, No. 5, pp. 681–693, 2007.
38. Wiley, B., Sun, Y., Xia, Y., “Synthesis of Silver Nanostructures with Controlled Shapes and Properties”, *Acc. Chem. Res.*, Vol. 40, No. 10, pp. 1067-1076, 2007.
39. Ru, E. L., Etchegoin, P. Principles of Surface Enhanced Raman Spectroscopy, Elsevier: Oxford, U.K., 2009.
40. Prucek, R., L. Kvitek and J. Hrbáč, “Silver Colloids-Methods of Preparation and Utilization”, *Acta Univ. Palacki. Olom. Chemica*, Vol. 43, pp. 7-27, 2004.
41. Chen, S. H. and D. L. Carroll, “Synthesis and characterization of truncated triangular silver nanoplate”, *Nano Lett.*, Vol. 2, No. 9, pp. 1003-1007, 2002.
42. Sun, Y. G. and Y. N. Xia, “Shape-controlled synthesis of gold and silver nanoparticles”, *Science*, Vol. 298, No. 5601, pp. 2176-2179, 2002.
43. Nadagouda, M.N., Speth, T.F., Varma, R.S., “Microwave-Assisted Green Synthesis of Silver Nanostructures”, *Accounts of Chemical Research*, Vol. 44, No. 7, pp. 469-478, 2011.
44. Lee P. C. and Meisel D., “Adsorption and surface-enhanced Raman of dyes on silver and gold sols”, *J. Phys. Chem.* Vol. 86, No. 17, pp. 3391-3395, 1982.

45. Aroca, R.F., Alvarez-Puebla, R.A., Pieczonka, N., Sanchez-Cortez, S., Garcia-Ramos, J.V., "Surface-enhanced Raman scattering on colloidal nanostructures", *Advances in Colloid and Interface Science*, Vol. 116, pp. 45-61, 2005.
46. Culha, M., Kahraman, M., Cam, D., Sayin, I., and Keseroglu, K., "Rapid identification of bacteria and yeast using surface-enhanced Raman scattering", *Surface and Interface Analysis*, Vol. 42, No. 6-7, pp. 462-465, 2010.
47. Saponjic, Z., Vodnik, V., Potkonjak, B., Jovancic, P., Nedeljkovic J. and Radetic, M., "The influence of silver content on antimicrobial activity and color of cotton fabrics functionalized with Ag nanoparticle", *Carbohydrate Polymers*, Vol. 78, No. 3, pp. 564-569, 2009.
48. Ghosh, S., S. Yadav and N. Reynolds, "Antibacterial properties of cotton fabric treated with silver nanoparticles", *Journal of the Textile Institute*, Vol. 101, No. 10, pp. 917-924, 2010.
49. Sun, T. and K. Seff, "Silver Clusters and Chemistry in Zeolites", *Chem. Rev.*, Vol. 94, No. 4, pp. 857-870, 1994.
50. Holme, D. J., Peck, H., *Analytical Biochemistry*, Printice Hall, 3rd Edition, p. 36, 1998.
51. Ujjal Kumar Sur, "Surface-Enhanced Raman Spectroscopy Recent Advancement of Raman Spectroscopy", *Resonance*, Vol. 15, No. 2, pp. 154-164, 2010.
52. Kelf, T., "Surface Enhanced Raman Spectroscopy", <http://www.timkelf.com/Research/ResearchSERS.html>, [retrieved 12 January 2012].
53. Raman C.V., and Krishnan K.S. "A New Type of Secondary Radiation", *Nature*, Vol. 121, No. 3048, pp. 501-502, 1928.

54. Landsberg and Mandelstam, "Über die Lichtzerstreuung in Kristallen", *Zeitschrift für Physik*, Vol. 50, No. 11-12, pp. 769-780, 1928.
55. Fleischman, M., Chang, B.H., "Oxygen absorption by intact red blood cells", *Federation Proceedings*, Vol. 33, No. 3, p. 1, 1974.
56. Wright, A., Gabaldon, J., Burckel, D.B., Jiang, Y.-B., Tian, Z.R., Liu, J., Brinker, C.J., Fan, H., "Hierarchically organized nanoparticle mesostructure arrays formed through hydrothermal self-assembly", *Chemistry of Materials*, Vol. 18, No. 13, pp. 3034-3038, 2006.
57. Kambhampati, P., and Campion, A., "Chemical Enhancement in Surface Enhanced Raman Scattering", *Proceedings of the XVIth International Conference on Raman Spectroscopy*, Wiley Interscience, New York, 1998.
58. Moskovits, M., "Surface-enhanced Raman spectroscopy: a brief retrospective", *J. Raman Spectrosc.*, Vol. 36, No. 6-7, pp. 485-496, 2005.
59. Han X. X., Zhao B., and Ozaki Y., "Surface-enhanced Raman scattering for protein detection", *Anal. Bioanal. Chem.*, Vol. 394, No. 7, pp. 1719–1727, 2009.
60. Stewart, S. and Fredericks, P. M., "Surface-enhanced Raman spectroscopy of peptides and proteins adsorbed on an electrochemically prepared silver surface", *Spectrochim. Acta, Part A*, Vol. 55, No. 7-8, pp. 1615–1640, 1999.
61. Zhang, D., Xie Y., Mrozek M. F., Ortiz C., Davisson V. J. and Ben-Amotz D., "Raman detection of proteomic analytes", *Anal. Chem.*, Vol. 75, No. 21, pp. 5703–5709, 2003.
62. Han X. X., Huang G. G., Zhao B. and Ozaki Y., "Label-Free Highly Sensitive Detection of Proteins in Aqueous Solutions Using Surface-Enhanced Raman Scattering", *Anal. Chem.*, Vol. 81, No. 9, pp. 3329–3333, 2009.

63. Kahraman M., Sur I. and Culha M., “Label-free detection of proteins from self-assembled protein-silver nanoparticle structures using surface-enhanced Raman scattering”, *Anal. Chem.*, Vol. 82, No. 18, pp. 7596-7602, 2010.
64. Bell, S. E. J., Sirimuthu, N. M. S., “Surface-enhanced Raman spectroscopy (SERS) for sub-micromolar detection of DNA/RNA mononucleotides”, *J. Am. Chem. Soc.*, Vol. 128, No. 49, pp. 15580–15581, 2006.
65. Yuan, W., Ho, H. P., Lee, R. K. Y., Kong, S. K., “ Surface-enhanced Raman scattering biosensor for DNA detection on nanoparticle island substrates”, *Appl. Opt.*, Vol. 48, No. 22, pp. 4329–4337, 2009.
66. Culha, M., Stokes, D., Allain, L. R., Vo-Dinh, T., “Surface-Enhanced Raman Scattering Substrate Based on a Self-Assembled Monolayer for Use in Gene Diagnostics”, *Anal. Chem.*, Vol. 75, No. 22, pp. 6196–6201. 2003.
67. Cao, Y. C., Jin, R., Mirkin, C. A., “Nanoparticles with Raman spectroscopic fingerprints for DNA and RNA detection”, *Science*, Vol. 297 No. 5586, pp. 1536–1540, 2002.
68. Kahraman, M., Zamaleeva, A. I., Fakhrullin, R. F., Culha, M., “Layer-by-layer coating of bacteria with noble metal nanoparticles for surface-enhanced Raman scattering”, *Anal. Bioanal. Chem.*, Vol. 395, No. 8, 2559-2567, 2009.
69. Culha, M., Adiguzel, A., Yazici, M. M., Kahraman, M., Sahin, F., Gulluce, M., “Characterization of Thermophilic Bacteria Using Surface-Enhanced Raman Scattering”, *Appl. Spectrosc.*, Vol. 62, No. 11, pp. 1226–1232, 2008.
70. Kahraman, M., Yazici, M. M., Sahin, F., Culha, M., “Convective assembly of bacteria for surface-enhanced Raman scattering”, *Langmuir*, Vol. 24, No. 3, 894–901, 2008.

71. Sayin, I., Kahraman, M., Sahin, F., Yurdakul, D., Culha, M., “Characterization of Yeast Species Using Surface-Enhanced Raman Scattering”, *Appl. Spectrosc.*, Vol. 63, No. 11, pp. 1276–1282, 2009.
72. Shanmukh, S., Jones, L., Driskell, J., Zhao, Y. P., Dluhy, R., Tripp, R. A., “Rapid and Sensitive Detection of Respiratory Virus Molecular Signatures Using a Silver Nanorod Array SERS Substrate”, *Nano Lett.*, Vol. 6, No. 11, pp. 2630–2636, 2006.
73. Alexander, T. A., “Development of Methodology Based on Commercialized SERS-Active Substrates for Rapid Discrimination of Poxviridae Virions”, *Anal. Chem.*, Vol. 80, No. 8, pp. 2817–2825, 2008.
74. Kneipp, J., Kneipp, H., Wittig, B., Kneipp, K., “Novel optical nanosensors for probing and imaging live cells”, *Nanomed. Nanotechnol. Biol. Med.*, Vol. 6, No. 2, pp. 214–226, 2010.
75. Tang, H. W., Yang, X. B. B., Kirkham, J., Smith, D. A., “Chemical probing of single cancer cells with gold nanoaggregates by surface-enhanced Raman scattering”, *Appl. Spectrosc.*, Vol. 62, No. 10, pp. 1060–1069, 2008.
76. Kneipp, K., Haka, A. S., Kneipp, H., Badizadegan, K., Yoshizawa, N., Boone, C., Shafer-Peltier, K. E., Motz, J. T., Dasari, R. R., Feld, M. S., “Surface-enhanced raman spectroscopy in single living cells using gold nanoparticles”, *Appl. Spectrosc.*, Vol. 56, No. 2, pp. 150–154, 2002.
77. Cao, Y. C., Jin, R., Nam, J.-M., Thaxton, C. S., Mirkin, C. A. J., “Raman Dye-Labeled Nanoparticle Probes for Proteins“, *Am. Chem. Soc.*, Vol. 125, No.48, pp. 14676-14677, 2006.
78. Grubisha, D. S., Lipert, R. J., Park, H.-Y., Driskell, J., Porter, M. D., “Femtomolar Detection of Prostate-Specific Antigen: An Immunoassay Based on Surface-Enhanced Raman Scattering and Immunogold Labels“, *Anal. Chem.*, Vol. 75, No. 21, pp. 5936-5943, 2003.

79. Zhou, Z., Huang, G.G., Kato, T., Ozaki, Y. "Experimental parameters for the SERS of nitrate ion for label-free semi-quantitative detection of proteins and mechanism for proteins to form SERS hot sites: A SERS study", *J. Raman Spectrosc.*, Vol. 42, No. 9, pp. 1713-1721, 2011.
80. Yang, X., Gu, C., Qian, F., Li, Y., Zhang, J.Z., "Highly sensitive detection of proteins and bacteria in aqueous solution using surface-enhanced Raman scattering and optical fibers", *Anal. Chem.*, Vol. 83, No. 15, pp. 5888-5894, 2011.
81. Culha, M., Altunbek, M., Keskin, S., Saatci, D., "Manipulation of Silver Nanoparticles in a droplet for label-free detection of biological molecules using surface-enhanced Raman scattering", *Proc. SPIE.*, 7911, Article number 791102, 2011.
82. Keskin, S., Kahraman, M., Culha, M., "Differential separation of protein mixtures using convective assembly and label-free detection with surface enhanced Raman scattering", *Chem. Commun.*, Vol. 47, No. 12, pp. 3424-3426, 2011.
83. Zhang, J., Qu, S., Zhang, L., Tang, A., Wang, Z., "Quantitative surface enhanced Raman scattering detection based on the "sandwich" structure substrate", *Spectrochim. Acta, Part A*. Vol. 79, No. 3, pp. 625-630, 2011.
84. Shen, X., Ho, C-M., Wong, T-S., "Minimal size of coffee ring structure", *J. Phys. Chem. B.*, Vol. 114, No. 16, pp. 5269-5274, 2010.
85. Hu, H. and Larson, R. G., "Marangoni effect reverses coffee-ring depositions", *J. Phys. Chem. B.*, Vol. 110, No. 14, pp. 7090-7094, 2006.
86. Jiang, J., Bosnick, K., Maillard, M., Brus, L., "Single molecule Raman spectroscopy at the junctions of large Ag nanocrystals", *J. Phys. Chem. B.*, Vol. 107, No. 37, pp. 9964-997, 2003.

87. Nelson, D. L. and Cox, M. M., “*Principles of Biochemistry*”, Lehninger, 2004.
88. Kneipp K., Kneipp H. Corio P., Brown S. D. M., Shafer K., Motz J., Perelman L. T., Hanlon E. B., Marucci A., Dresselhaus G., Dresselhaus, M. S., “Surface-Enhanced and Normal Stokes and Anti-Stokes Raman Spectroscopy of Single-Walled Carbon Nanotubes“, *Phys. Rev. Lett.*, Vol. 84, No. 15, pp. 3470–3473, 2010.
89. Weitz, D. A., Oliveria M., “Fractal structures formed by kinetic aggregation of aqueous gold colloids“, *Phys. Rev. Lett.*, Vol. 52, No. 16, pp. 1433–1436, 1984.
90. Adachi E., Dimitro A.S., Nagayama K., “Stripe patterns formed on a glass surface during droplet evaporation”, *Langmuir*, Vol. 11, No. 4, pp. 1057–1060, 1995.
91. Shmuylovich L., Shen A. Q. & Stone H. A., “Surface morphology of drying latex films: multiple ring formation”, *Langmuir*, Vol. 18, No.9, pp. 3441-3445, 2002.
92. Dussan V.E.B., “On the spreading of liquids on solid surfaces: Static and. dynamic contact lines”, *Annu. Rev. Fluid Mech.*, Vol. 11, pp. 371-400, 1979.
93. Rio E., Daerr A., Lequeux F., Limat L., “Moving contact line of colloidal suspension in the presence of drying”, *Langmuir*, Vol. 22, No. 7, pp. 3186-3191, 2006.
94. Das, G., Gentile, F., Coluccio, M.L., Perri, A. M., Nicastrì, A., Mearini, F., Cojoc, G., Candeloro, P., Liberale, C., De Angelis, F., Di Fabrizio, E. “Principal component analysis based methodology to distinguish protein SERS spectra“, *J. Mol. Struct.*, Vol. 993, No. 1-3, pp. 500-505, 2011.
95. Das, G., Mearini, F., Gentile, F., De Angelis, F., Mohan Kumar, H. G., Candeloro, P., Liberale, C., Cuda, G., Di Fabrizio, E., “Nano-patterned SERS substrate: Application for protein analysis vs. temperature”, *Biosens. Bioelectron.*, Vol. 24, No. 6, pp. 1693-1699, 2009.

96. Dong, O., Lam, D. C. C., “Silver nanoparticles as surface-enhanced Raman substrate for quantitative identification of label-free proteins”, *Mater. Chem. Phys.*, Vol. 126, No. 1-2, pp. 91-96, 2011.
97. Stone, N., Kendall, C., Shepherd, N., Crow, P., and Barr, H., “Near-infrared Raman spectroscopy for the classification of epithelial pre-cancers and cancers”, *J. Raman Spectrosc.*, Vol. 33, No. 7, pp. 564–573, 2002.
98. Shetty, G., Kendall, C., Shepherd, N., Stone, N., Barr, H., “Raman spectroscopy: elucidation of biochemical changes in carcinogenesis of oesophagus”, *British Journal Of Cancer*, Vol. 94, No. 10, pp. 1460-1464, 2006.
99. Chan, J.W., Taylor, D.S., Zwerdling, T., Lane, S.T., Ihara, K., and Huser, T., “Micro-Raman spectroscopy detects individual neoplastic and normal hematopoietic cells”, *Biophys. J.* Vol. 90, No. 2, pp. 648–656, 2006.
100. Cheng, W.-T., Liu, M.-T., Liu, H.-N., and Lin, S.-Y., “Micro-Raman spectroscopy used to identify and grade human skin pilomatrixoma”, *Microsc. Res. Tech.*, Vol. 68, No. 2, pp. 75–79, 2005.
101. Naumann, D., “Infrared and NIR Raman spectroscopy in medical microbiology”, *Proc. SPIE.*, 3257, pp. 245–257, 1998.
102. Lau, D.P., Huang, Z., Lui, H., Man, C.S., Berean, K., Morrison, M.D., and Zeng, H., “Raman spectroscopy for optical diagnosis in normal and cancerous tissue of the nasopharynx - Preliminary findings”, *Lasers in Surgery and Medicine.*, Vol. 32, No. 3, pp. 210–214, 2003.
103. Gniadecka, M., Wulf, H.C., Mortensen, N.N., Nielsen, O.F., and Christensen, D.H., “Diagnosis of basal cell carcinoma by Raman spectroscopy”, *J. Raman Spectrosc.*, Vol. 28, No. 2-3, pp. 125–129, 1997.

104. Stone, N., Kendall, C., Smith, J., Crow, P., and Barr, H., "Raman spectroscopy for identification of epithelial cancers", *Faraday Discuss.*, Vol. 126, pp. 141–157, 2004.
105. Lakshimi, R.J., Kartha, V.B., Krishna, C.M., Solomon, J.G.R., Ullas, G., and Uma Devi, P., "Tissue Raman spectroscopy for the study of radiation damage: Brain irradiation of mice", *Radiat. Res.*, Vol. 157, No. 2, pp. 175–182, 2002.
106. Dukor, R.K., "Vibrational spectroscopy in the detection of cancer", *Biomed. Applications.*, Vol. 5, pp. 3335–3359, 2002.
107. Yang, K. H., Liu, Y. C. and Hsu, T. C., "Interesting substrate-temperature dependence on surface-enhanced Raman scattering", *Journal Of Electroanalytical Chemistry*, Vol. 632, No. 1-2, pp. 184-191, 2009.
108. Lang, X. Y., Guan, P. F., Zhang, L., Fujita, T. and Chen, M. W., "Characteristic Length and Temperature Dependence of Surface Enhanced Raman Scattering of Nanoporous Gold", *Journal of Physical Chemistry C*, Vol. 113, No. 25, pp. 10956-10961, 2009.
109. Liu, Y. C.; Yang, K. H. and Hsu, T. C., "Improved Surface-Enhanced Raman Scattering Performances on Silver-Silica Nanocomposites", *Journal of Physical Chemistry C*, Vol. 113, No. 19, pp. 8162-8168, 2009.